Journal of Wind Engineering & Industrial Aerodynamics 166 (2017) 1–19

Contents lists available at ScienceDirect

Journal of Wind Engineering and Industrial Aerodynamics

journal homepage: www.elsevier.com/locate/jweia

A wind-tunnel methodology for assessing the slipstream of high-speed trains

J.R. Bell[a,*], D. Burton[a], M.C. Thompson[a], A.H. Herbst[b], J. Sheridan[a]

[a] Department of Mechanical and Aerospace Engineering, Monash University, Clayton, Victoria 3800, Australia
[b] Centre of Competence for Aero- and Thermodynamics, Bombardier Transportation, Vasteras, Sweden

ARTICLE INFO

Keywords:
Slipstream
High-speed train
Wake
Gust

ABSTRACT

A 1/10th-scale wind-tunnel technique for assessing the slipstream of high-speed trains (HST) is assessed through comparison to full-scale field and 1/25th-scale moving-model experimental results of an Inter-City Express 3 (ICE3) – a HST in operation throughout Europe and Asia – with the view of applying the wind-tunnel methodology for checking regulatory compliance in the design phase of a HST. The effect of the experimental limitations inherent in a wind-tunnel slipstream methodology: the presence of a stationary floor, reduced length of the model, limited test-section size and ground-fixed frame-of-reference are also investigated. Subsequently, recommendations for the use of wind-tunnel and moving model methodologies for assessing the slipstream of prototype HSTs with an applied, industrial aerodynamics focus, are made.

1. Introduction

Slipstream is the air flow induced by a vehicle's movement. In practice, it is measured at a fixed distance from the vertical centreplane of the train. It is an important consideration for the aerodynamic performance but also for the safe operation of high-speed trains (HSTs). Such flows can be hazardous to commuters waiting at platforms and to track-side workers (Pope, 2007) due to the significant pressure forces. Regulations are in place that limit the magnitude of slipstream velocities a HST can induce. A high-speed train must adhere to the slipstream limits of the European Railway Agency's (ERA) Technical Specifications for Interoperability (TSI) in order to operate in Europe (ERA, 2008). The TSI are informed by the European Committee for Standardizations regulations, herein referred to as the European Norms (EN) (CEN, 2009), which cover practices for full-scale and scaled experiments, as well as numerical simulations.

The largest *slipstream* velocities are found to occur in the wake of a HST (Baker, 2010; Baker et al., 2012a; Bell et al., 2014, 2015). The authors have previously associated high slipstream velocities in the wake to the presence of a streamwise vortex pair that exist in the time-averaged flow topology (Bell et al., 2014). The contribution of these vortices to characterising the slipstream of a HST has also been identified by preceding research (Baker, 2010; Weise et al., 2006; Muld et al., 2012a). The vortices move downwards and outwards beyond the passage of the train causing the largest slipstream velocities to exist where people or infrastructure may be affected. The peak instantaneous slipstream velocities also occur in the near wake, however the magnitude and location of these peaks has been shown to be inconsistent in scaled moving-model experiments (Baker, 2010; Bell et al., 2015) and numerical investigations (Muld et al., 2012b; Pii et al., 2014; Hemida et al., 2014). Previous work by the authors has postulated that this is caused by periodic spanwise oscillations of the vortex pair, caused by merging and interaction of von Karman-type vortex shedding from the vehicle's side (Bell et al., 2014, 2016a, 2016b), as illustrated in Fig. 1. A methodology for measuring the slipstream of a HST must therefore be able to measure the effects of these transient wake characteristics to properly predict the slipstream.

For the first time, the slipstream of the same ICE3 HST geometry is presented and directly compared from three different experiment methodologies: full-scale, scaled moving-model and scaled wind tunnel. Such analysis provides quantifiable insight into the level of confidence in the wind-tunnel methodologies slipstream assessment of HSTs in the prototype phase. The wind-tunnel methodology has previously been shown to be particularly useful in providing insight into the causes of high slipstream velocities (Weise et al., 2006; Bell et al., 2014, 2016a, 2016b). However, until now, insight into the accuracy of slipstream results achievable by the methodology has been limited. The accuracy of the slipstream results achievable using a scaled moving model methodology has previously been published (Bell et al., 2015). This work, part of a collaboration between Monash University and Bombardier Transportation, contributes to the establishment of accurate and feasible experimental methodologies for assessing the

* Corresponding author.
E-mail address: james.bell@monash.edu (J.R. Bell).

http://dx.doi.org/10.1016/j.jweia.2017.03.012
Received 28 July 2016; Received in revised form 8 March 2017; Accepted 25 March 2017

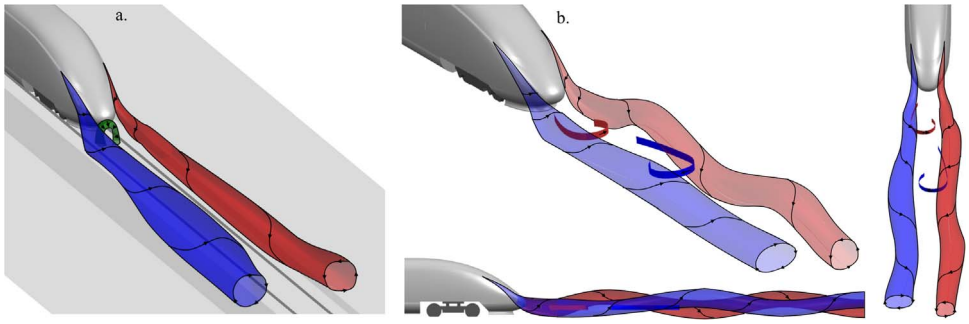

Fig. 1. (a) Time-averaged wake topology. (b) Unsteady wake topology (first appeared in Bell et al., 2016a and Bell et al., 2016b respectively.)

slipstream of HSTs. Ultimately, it is hoped that the developed methodologies are utilised in the design process of future generations of HSTs.

2. Methodology

2.1. Experimental model

A 1/10th-scale simplified version of a Deutsche Bahn Inter-City-Express 3 (ICE3) high-speed train is the model investigated in the presented work. The external shape, and thus external aerodynamics, are the same as the Siemens Velaro HST. This HST is in operation throughout Germany, Netherlands, Belgium, Austria, Switzerland, Denmark, France, Spain, Turkey, Russia, and China. The HST Computer-Aided Design (CAD) model geometry is freely available from the TC 256 Secretariat held by the DIN Standards Railway Committee (FSF) (FSF, 2004). The availability of the ICE3 geometry, its wide use throughout the world, and its modern aerodynamic shape that is similar to other current HSTs in operation makes it an ideal geometry for assessing the accuracy of experimental methodologies for predicting the slipstream of typical of modern HSTs.

The ICE3 1/10th-scale wind-tunnel model (Fig. 2a) measured $5.2 \times 0.3 \times 0.4$ m ($L \times W \times H$), with a cross sectional area of ≈ 0.12 m^2. The model had four sets of bogies, no pantographs, no inter-carriage gaps and no heating, ventilation and air conditioning (HVAC), as the essential geometry—the gross external shape—is the focus of this investigation. The model was supported by 6 pairs of $0.05H$ (20 mm) diameter cylindrical supports in line with the wheels in the bogies.

The length of the ICE3 model was altered to achieve L/H ratios of 5.75, 8.25, 10.5, and 13, with larger L/H simulated by augmenting the boundary layer development over the surface of the train in three ways: a 0.035H (14 mm) high fence trips (Tr), and 0.125H and 0.25H (50, 100 m) high spire trips (Sp), placed around the circumference of the model (Fig. 3). These trips were placed 2.5H from the train's nose. The width-to-height ratio of the spires was 0.3 with no gap between tips. The authors have previously presented the effect L/H has on the wake and pressure distribution of the same model in this work (Bell et al., 2014). Boundary layer augmentation in a similar manner to that applied here has also been investigated on a moving-model experiment by Sima et al. (2016).

2.2. Wind-tunnel experimental setup

The experiment was performed in the closed circuit Monash University 1.4 MW wind tunnel (Fig. 4). The wind tunnel is capable of wind speeds between 5 and 65 m/s utilizing fixed-pitch axial fans, driven by a 1.4 MW quad-motor system. The experimental setup (Fig. 5) models a train travelling on a straight track over flat ground with no crosswind which aims to isolate the slipstream characteristics generated by the train's essential generic geometry in an ideal environment. The coordinate system adopted is presented in Fig. 5. Streamwise position, x, is normalized by the model height (H), with x=0 corresponding to the position of the tail, as is the practice in general ground-vehicle aerodynamics (Bearman et al., 1988; Krajnović and Davidson, 2005). In addition, literature has indicated that the near-wake is dominated by the tail geometry (Morel, 1980; Muld et al., 2012b). Cross-stream position, y, is normalized by the model width (W), with y=−1/2 corresponding to the left vertical edge and y=1/2 to the right edge. Vertical position, z, is normalized by model height, with z=0 corresponding to the top of the rails (TOR).

The 3/4 open test section measuring $12 \times 4 \times 2.5$ m^3 ($L \times W \times H$) was fitted with a 0.5 m (1.2H) high splitter plane to reduce ground boundary layer effects, resulting in a cross-sectional area above the splitter plane of 8.0 m^2. A 1/10th-scale *Single Track Ballast and Rail* (STBR) ground configuration (Fig. 5b) was included in the setup, with height of 100 mm (0.24H) and upper and lower widths of 300 mm (1 W) and 555 mm (1.85 W) respectively, adhering to the EN (CEN, 2009). The leading edge of the STBR had a front angle equivalent to the side angle (37°) swept 180°. Velocity measurements established no separation occurred over the leading edge of the STBR. The model was supported above the STBR by 6 pairs of 0.05H (20 mm)diameter cylindrical supports, in line with the wheels in the bogies, at x=−12, −8.5, −6.5, −4.5, −3.5 and −1.5H. The maximum blockage ratio was ≈2% above the splitter plate, including blockage due to the traverse and STBR. Thus, blockage effects are expected to be minimal, and no blockage corrections were applied. The approximate turbulence intensity (I_{uvw}) above the wind tunnel boundary layer was 1.6%.

The measured displacement thickness of the boundary layer – a result of the stationary floor – was $\delta^*/H = 0.006$ and 0.035 at the model's nose and tail positions, respectively, in an empty tunnel above

Fig. 2. The Inter-City-Express 3 high-speed train geometry investigated: (a) 1/10th-scale wind-tunnel model, (b) 1/25th-scale moving-model, (c) full-scale operational train (Photo provided courtesy of Bombardier Transportation).

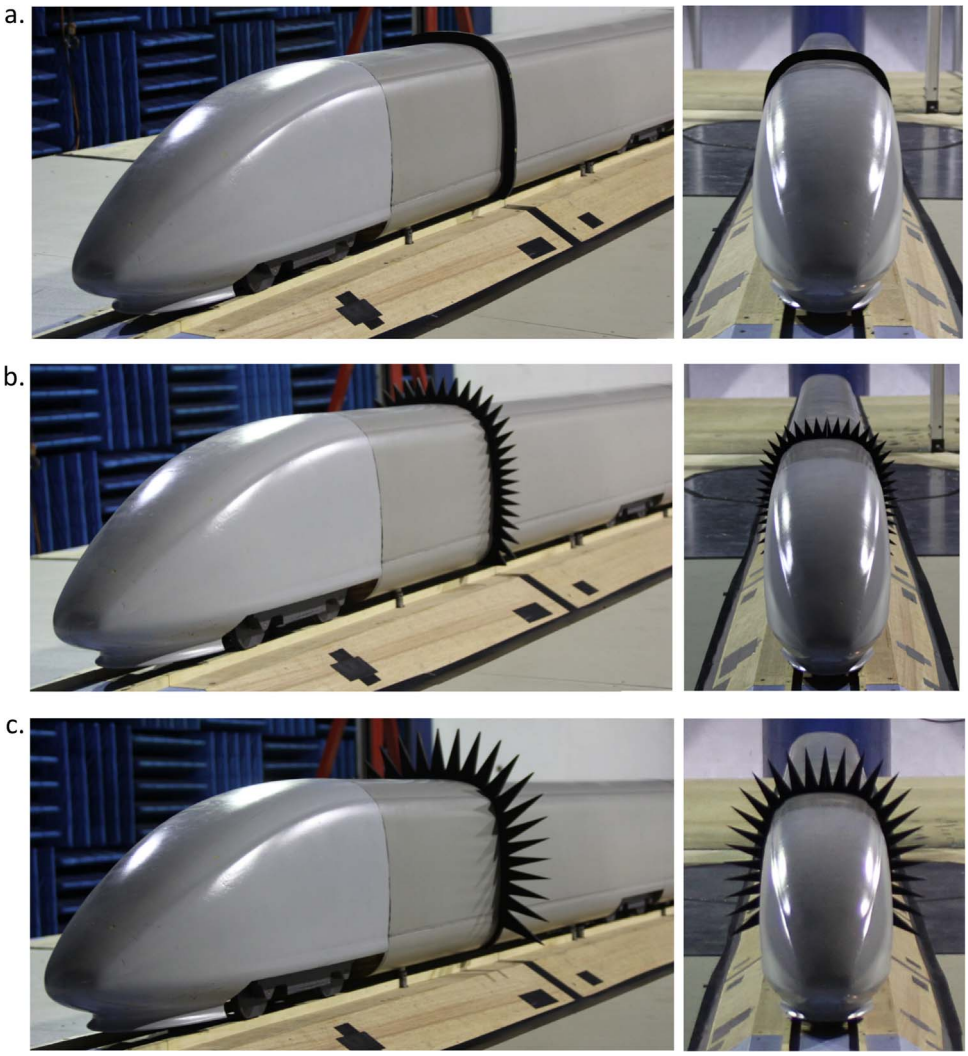

Fig. 3. Boundary layer augmentation devices, applied at x=2.5H (1 m from the models nose). (a) 0.25H (25 mm) fence trip, (b) 0.125H (50 mm) spires, (c) 0.25H (100 m) spires.

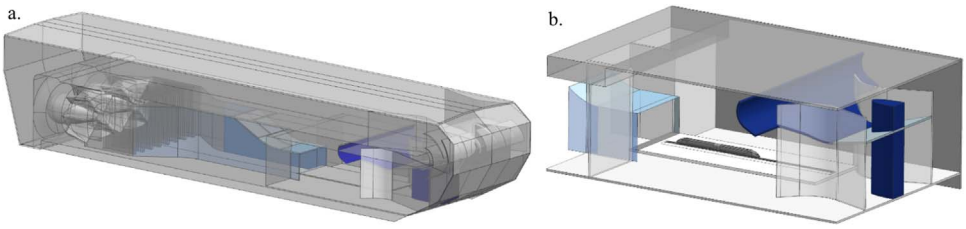

Fig. 4. (a) The Monash University 1.4 MW closed-return wind tunnel. (b) 1:10th-scale ICE3 model in the 3/4 open-jet test section. A 600 mm high splitter plate (shown) was utilised to reduce the ground boundary layer.

the splitter plate. The side and roof boundary layers were measured and analysed as 2D boundary layers for simplicity as previous researchers have done (Baker, 2010; Muld et al., 2013). The displacement thicknesses of the boundary layer at $x = -2.5$, z=0.5, at the side, $x = -2.5$, y=0 on the roof, were $\delta^*/H = 3.12 \times 10^{-2}$ and 2.82×10^{-3}, corresponding to momentum thicknesses of $\theta/H = 2.50 \times 10^{-2}$ and 2.70×10^{-3} respectively.

Sensitivity of the results to Reynolds number over the range Re_W=0.5 × 10^6–1 × 10^6, using width as the characteristic length, corresponding to freestream velocities of 25–48 m/s, is discussed in the results section, however this is still significantly smaller than the typical full-scale Reynolds number of 17×10^6 (corresponding to a full-scale train travelling at 300 km/h).

2.2.1. 4-Hole Cobra probe measurements

Measurements were taken with a 4-hole dynamic-pressure probe (cobra probe). Specifications indicate that the cobra probe is capable of determining velocities with the accuracy of ± 1 m/s within a ± 45° cone angle; however, it is not capable of measuring reversed flow (Hooper and Musgrove, 1997). Despite this, an indication of the percentage of flow that is outside its calibrated cone of acceptance is provided by the probes accompanying software, and in all cases reported >95% of measurements were within the cone of acceptance. The cobra probe, consisting of the set of tubes and four differential pressure transducers, is specified by the manufacturer (TFI) to have a frequency response above 2000 Hz.

To obtain slipstream profiles, two cobra probes measured were mounted with 0.25H (100 mm) spacing and were moved using a

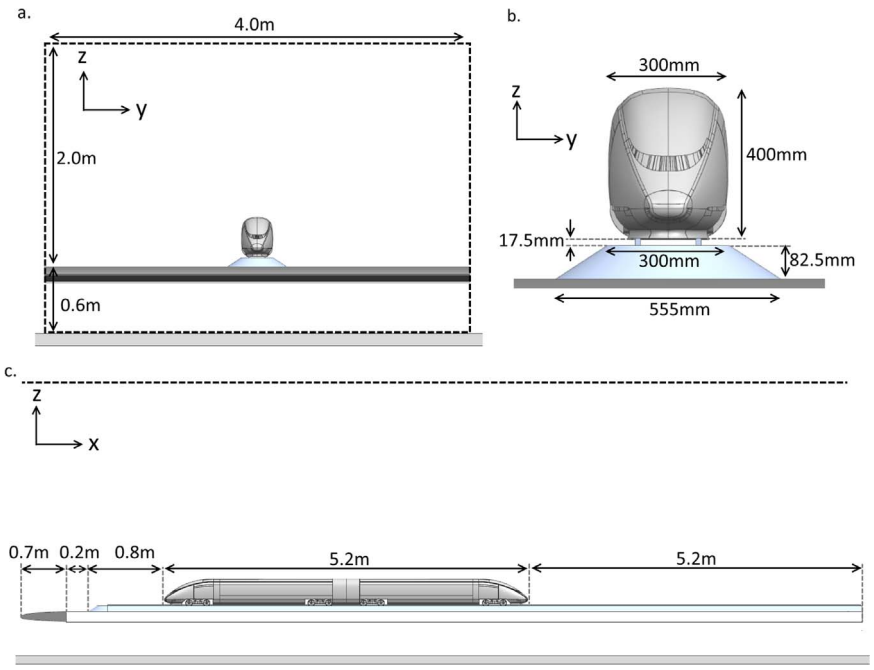

Fig. 5. The 1:10th-scale ICE3 model in the 3/4 open-jet test section of the Monash University 1.4 MW wind tunnel. A 600 mm high splitter plate was utilised to reduce the ground boundary layer.

Fig. 6. The experimental configuration of the cobra probes mounted on streamlined and balanced arms, and moved with a computer controlled traverse. This setup was used to obtain streamwise measurements to develop slipstream profiles.

computer controlled mechanical traverse. The mounting configuration of the two cobra probes (Fig. 6) was designed to reduce interference with measurements and minimize both structural and aerodynamic vibrations. The traverse was also streamlined with curved high-density foam blocks over its bluff forward facing edges. Streamwise (x direction) sweeps with a high spatial resolution $0.05H$ (20 mm), were performed at $x = -15H$ (upstream of the nose) to $10H$ (in the wake), at $y = 2(W/2)$, z=0.05, 0.15, 0.30 and $0.36H$ above the top of rail (TOR). The specific heights z=$0.05H$ above TOR & z=$0.36H$ above TOR are equivalent to the TSI (ERA, 2008) 'track-side' and 'platform' heights (z=0.2 m and z=1.44 m). The positions measured are representative of the locations where people or infrastructure might be influenced by the induced flow around the vehicle. These also correspond to the positions at which a HST is assessed for slipstream holmologation in the TSI (ERA, 2008) and EN (CEN, 2009) regulations.

The velocities measured by the cobra probe in the wind tunnel are obtained taking point-wise measurements and have a train-fixed frame-of-reference (TF). In contrast, full-scale field experiments assessing the slipstream of HSTs have been performed using ground-fixed probes, most commonly ultrasonic anemometers (Baker et al., 2012a, 2012b), in the ground-fixed frame-of-reference (GF), the perspective of a stationary observer. To account for this difference, the component of the measured velocity (in m/s denoted with a * in the wind tunnel experiments in the x direction (u^*) was converted to GF and normalized against the freestream velocity, u_∞:

$$u_{GF} = 1 - \frac{u^*_{TF}}{u_\infty}. \tag{1}$$

The measured components of velocity in the y direction (v^*) and z direction (w^*) were normalized against the freestream velocity (u_∞):

$$v = \frac{v^*}{u_\infty}, \quad w = \frac{w^*}{u_\infty}. \tag{2}$$

The resultant of the u_{GF} and v components of velocity, $\sqrt{u_{GF}^2 + v^2}$ is referred to as 'horizontal velocity' herein, and is of primary focus as it presents safety risk of destabilising a person, whereas the w component of velocity is proposed not to present a safety risk.

Time-averaged profiles of point-wise measurements are presented for the wind-tunnel results, such results are statistically equivalent to ensemble averaged results calculated from individual runs measured by the moving-model and full-scale experiments as the train moves past measurement equipment.

Results are presented raw, and with a moving-average applied equivalent to a 1 s window full-scale at $u_t = 300$ km/h, as this type of moving-average is applied to each individual run during processing for regulatory slipstream risk assessment.

2.3. Moving-model experimental setup

The moving-model experiment was performed at Deutsches Zentrum für Luft- und Raumfahrt (DLR - German Aerospace Centre) Tunnel Simulation Facility (TSG), a moving model facility in Göttingen, Germany.

A 1/25 scale model of an ICE3 was used. Two pairs of light gates (with 0.35 m spacing between paired individuals and 6.0 m spacing between the two pairs) were used to determine the models velocity and acceleration, single hot wires were used to measure the induced velocity. The model was a 3 car, 2.7 m (L/H=16) long model fired at 32 m/s (Re=250,000, width as characteristic length). Further details of the moving-model methodology and results have previously been published by the authors (Bell et al., 2015).

The velocity measured in the moving-model experiment was converted from the time domain to the spatial domain utilizing the scaled model train's speed, u_t. In full-scale field experiments, a 1 s moving average in the time domain is equivalent to an 83.3 m (20.8H) moving-average in the spatial domain, as the train is travelling 83.3 m/s (300 km/h). An equivalent spatial moving-average in the scaled experiment, considering the length-scale of 1/25, is 3.33 m (83.3/25). This ensures the same size flow structures were analysed in the scaled experiment compared to the full scale, all else being equal. This method of converting to the spatial domain utilising the model train speed, incorporates both the length and velocity scales, which is a higher level of detail to that suggested in the EN for scaled testing (CEN, 2009) which only accounts for length scale.

The applied moving-average is a lag-type, thus the value at $x = 0H$ is an average of $x = -20.8H$ to $x = 0H$. This causes the moving-average signal to appear to lag behind the raw (no moving-average applied) slipstream profiles. The EN does not specify what type of moving-average to apply (CEN, 2009). Thus, this basic type of moving-average was adopted and applied to all data presented (full-scale, moving-model and wind tunnel).

The two hot-wire probes S2 and S3 were located at $y = 2(W/2)$, $z = 0.05H$, and had longitudinal spacing of $x = 5H$ (0.8 m in the 1/25th-scaled experiment). This corresponds to 20 m full-scale which adheres to the full-scale specifications; TSI (ERA, 2008) and the EN (CEN, 2009) for measurement of the same run with multiple probes. By positioning two probes at the same y and z position, at a large enough longitudinal distance from each other, the number of runs measured are effectively multiplied. This technique is called 'run multiplication' and its validity for the moving-model experiment is provided in greater detail in Bell et al. (2015). Due to the distance between (2.0 m) and size of the probes (diameter of 0.005 m) and zero ambient wind, interference effects between the hot wires were assumed to be negligible. This resulted in 60 effective runs processed.

2.4. Full-scale experimental setup

The full-scale results presented are from field tests undertaken in Spain as part of Work Package 5 of the AeroTRAIN project. These results are from an 8 car, 200.3 m long Siemens Velaro S-103 high-speed train, and are a subset of data presented in Baker et al. (2012a, 2012b), Baker (2012). The external geometry of the S-103 is considered the same as the ICE3 geometry of the scaled wind-tunnel and moving models used in the respective experiments. The ground configuration was a double track with rock ballast.

Slipstream velocity was measured by a number of ultra-sonic anemometers with a sampling frequency of 265 Hz, corresponding to a spatial resolution of 0.3 m. This is larger than the 100Hz minimum required by the TSI and EN regulations.

For the direct comparison of slipstream results across thee methodologies, 60 of the 294 full-scale ICE3 runs available for processing were analysed. The 60 runs selected had the lowest ambient wind, u_{amb}, on the condition that the train speed (u_t) was greater than 78 m/s. This resulted in a range of $u_{amb} = 0.1 - 0.95$ m/s $\approx 0.01u_t$. Sensitivity of the full-scale slipstream results to run selection criteria is investigated in Section 3.3.3.

3. Time-averaged slipstream results

3.1. Wind-tunnel slipstream results

The slipstream results obtained from the wind tunnel measurements, and their specific processing are presented in this section prior to comparison to the full-scale and moving-model results in Section 3.2.

3.1.1. Time-average slipstream profiles

Streamwise velocity profiles along the vehicles side at $y = 2(W/2)$ and heights of z=0.05, 0.15, 0.30, 0.36H are presented in Fig. 7.

The average and standard deviation at each measured point in the wind-tunnel experiment are plotted as streamwise profiles. The local peaks in u velocity at the tail and nose are associated to the significant peaks in v velocity at these positions (Fig. 7b). This occurs as the flow is accelerated in the horizontal plane around the side curvature of the vehicle. This is more pronounced at the higher positions $z = 0.30H$ and $0.36H$ as the side curvature of the vehicle is greater at these heights. The larger near-wake peak of v at $z = 0.15H$ relative to other heights occurs as this is the location of the time-averaged streamwise vortex, specifically the lower edge, which contains high values of spanwise velocity (Bell et al., 2016a). Similarly, the higher relative value of w (Fig. 7c) at $z = 0.36H$ is explained by this location corresponding to the outer edge of the time-averaged streamwise vortex which exhibits high vertical velocity.

3.1.2. Standard deviation slipstream profiles

The standard deviation of the three components of velocity are presented in Fig. 7e, f, g. High levels of standard deviation are visible in the near-wake, slightly upstream of the peak in time-averaged velocities. The peak levels of standard deviation are higher for the u component ($\sigma_u = 0.08$) compared to the v and w components ($\sigma_{v,w} \approx 0.06$). Standard deviation is low elsewhere other than in the near wake. This agrees with findings showing high run-run deviation in the near-wake in full-scale (Sterling et al., 2008), scaled moving-model experimental results (Sterling et al., 2008; Bell et al., 2015) and numerical results (Hemida et al., 2014) in the literature.

3.1.3. Peak slipstream profiles

Slipstream profiles of the average horizontal velocity, $\sqrt{u^2 + v^2}$ and an estimate of the 95% confidence interval of the horizontal velocity $\sqrt{u^2 + v^2} + 2\sigma_{uv}$, a statistical representation of the peak instantaneous velocity, are presented in Fig. 7d and h respectively. These peak slipstream profiles represent the 95% confidence interval of the slipstream velocity with and without a 1 s moving-average applied. This assumes the velocity follows a normal distribution, which analysis has established that it does not (Bell et al., 2014, 2016a). However, this type of analysis reflects the individual run processing for regulatory slipstream risk assessment and is similar to that applied in the field of wind engineering for gust analysis that still provides an estimate of the peak values, just not necessarily exactly a 95% confidence interval.

In moving-model and full-scale experiments, the train moves past the measurement equipment. Thus the length of measurements is, in practice, restricted by the sampling time and also track length. In contrast, the maximum length of measurements achievable in a wind-

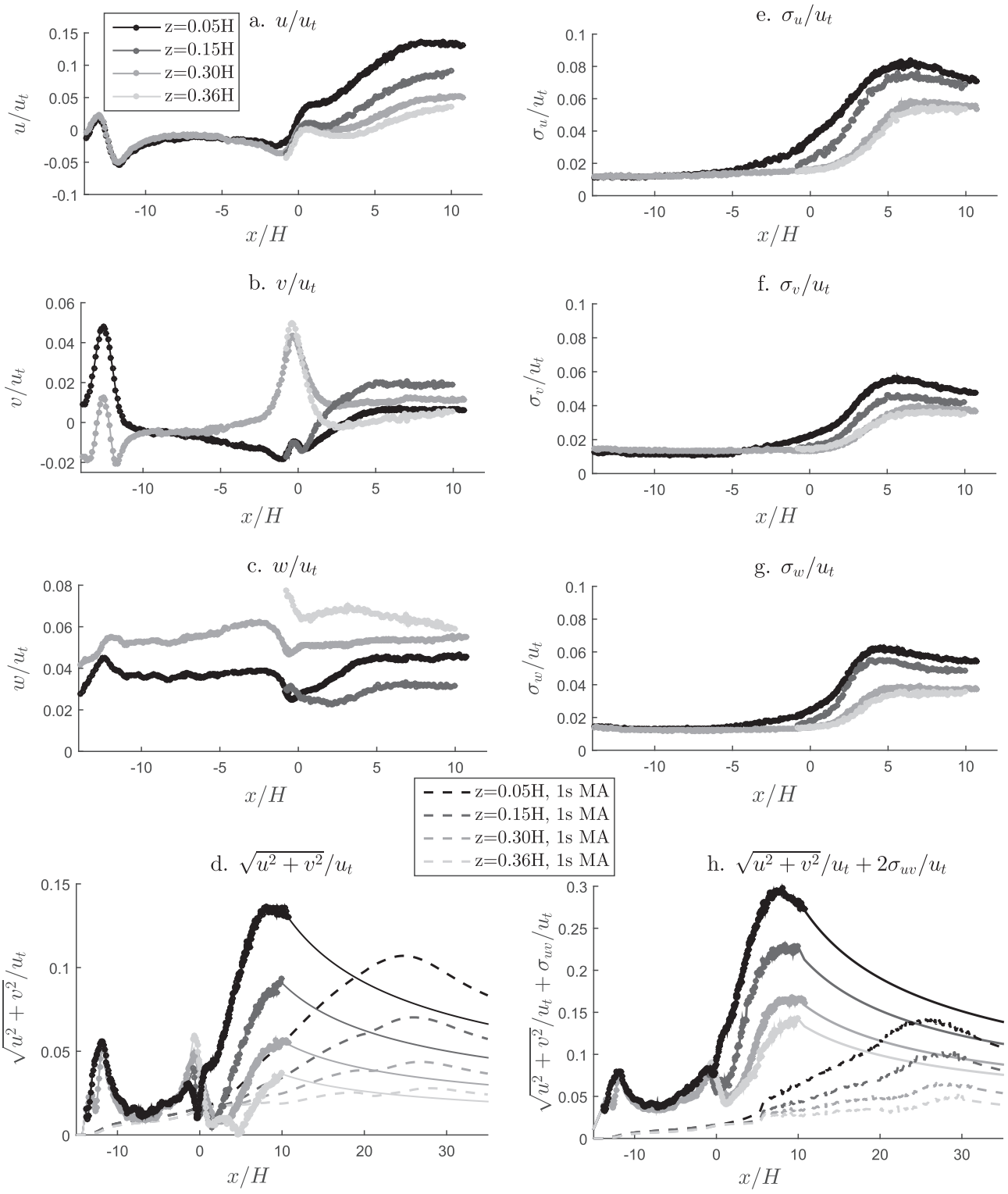

Fig. 7. Slipstream measured at $z = 0.05, 0.15, 0.30, 0.36H$. The three components of velocity: (a) u, (b) v, (c) w, and their respective standard deviation: (e) σ_u, (f) σ_v, (h) σ_w, the horizontal velocity] (d) $\sqrt{u^2+v^2}$, (h) $\sqrt{u^2+v^2}+2\sigma_{uv}$. Results with a 1 s equivalent Moving Average (MA) are indicated by dashed lines.

tunnel experiment is limited by the size of the test-section. In this case the length of the splitter plate allows a measurable length of $-15H > x < 10H$. Thus to aid in the comparison of results between methodologies, the decay of slipstream velocity beyond that measured, $x > 10H$ (denoted as a continuation of the respective lines, without specific marker points in Fig. 7d and h), was estimated using a power–law relationship:

$$u = \alpha(x)^n, \tag{3}$$

where α and n are characteristics dependant on the position measured and type of train.

This power–law relationship has been established by Baker et al. (2012a) as a good approximation of the decay of velocity in the wake of full-scale measurements of an ICE3 HST. This method is an extension to that of Baker (2001). The exponent, n for the full-scale ICE3 results

Table 1
Parameters for power-law estimation of slipstream horizontal velocity decay in the wake.

z/H	0.05	0.15	0.30	0.36
α	15.3	8.0	3.6	1.9
n	−0.57	−0.54	−0.50	−0.48

measured at $z = 0.05H\&0.36H$ by Baker et al. (2012a) were $n = -0.57$ and $n - 0.5$ respectively. These values were used as a starting point for applying the power law relationship to estimate the decay following the scaled wind tunnel results, the parameters of which are provided in Table 1.

The decay relationship was appended to the measured slipstream results up to $x = 250H$. Additionally, the slipstream upstream of that measured ($x < -15H$) was approximated by $\sqrt{u^2 + v^2} = 0$ up to $x = -250H$. These extrapolated sections of the results were added to allow the spatial average equivalent to a 1 s moving average to a slipstream profile over a larger streamwise distance and thus, provide a better representation of the slipstream being measured. A 1 s moving-average is applied in slipstream assessment regulated by the TSI & EN (ERA, 2008; CEN, 2009).

The equivalent spatial average of the 1 s moving-average applied to full-scale individual runs measured is simple to apply to the wind-tunnel average slipstream profile. A 1 s moving average at full-scale at 300 km/h corresponds to a $20.8H$ spatial moving average. This $20.8H$ moving-average was applied to the scaled wind tunnel experimental data and takes into account velocity, length and time-scales.

However, the application of the moving average to the wind-tunnel standard deviation profile is more complicated. For full-scale and moving-model results, the standard deviation (and the corresponding 95% confidence interval profiles with a 1 s moving-average) are calculated from individual runs with the 1 s moving-average applied. This is not possible with the wind-tunnel results as individual runs are not measured, and applying an equivalent spatial average to a standard deviation profile is not physically representative of the moving-model process. Instead, the time-series measured at each individual point in the wind-tunnel experiment was filtered with a scaled equivalent of a 1 s moving-average by considering the time, velocity and length-scales of the wind-tunnel and full-scale experiment:

$$time\ scale = \frac{full\ scale\ time}{wind\ tunnel\ time} = \frac{length\ scale}{velocity\ scale}, \tag{4}$$

$$velocity\ scale = \frac{full\ scale\ velocity}{wind\ tunnel\ velocity}, \tag{5}$$

$$length\ scale = \frac{full\ scale\ length}{wind\ tunnel\ length}, \tag{6}$$

where the characteristic length in this case is the respective heights of the scaled-model (0.4 m) and full-scale (4.0 m) trains. The velocity and length scales were used to calculate the time-scale which was then used to calculate a scaled equivalent of the 1 s moving-average applied at full-scale. This corresponded to a 0.237 s moving-average being applied to the wind-tunnel experiment when $u_\infty = 35$ m/s.

A profile of the standard deviation at each measured position of the filtered signals is more representative of the full-scale and moving-model processing of individual runs. The last step of the processing was to translate the 1 s moving-average equivalent standard deviation profile 20.8H in the x direction to simulate the 'lag' that occurs when applying a spatial moving average. This is equivalent of considering the measured standard deviation of the filtered individual points as occurring at 20.8 downstream of the measured position, using Taylors' theorem to relate the velocity and time to space.

The profiles of horizontal velocity, $\sqrt{u^2 + v^2}$, in Fig. 7d includes the measured and estimated data and the resulting moving-average equivalent of 1 s of the $\sqrt{u^2 + v^2}$ profiles.

Table 2
Comparison of key features of slipstream profiles between methodologies.

	uv_N [a]	uv_T [b]	$\widehat{uv}$	$\widehat{uv}_{1s\ MA}$	$\hat{\sigma}_{uv}$	$\widehat{\overline{uv} + \sigma_{uv}}$	$\widehat{\overline{uv} + \sigma_{uv}}_{1s\ MA}$
$z = 0.05H$							
WT	0.056	0.041	0.136	0.107	0.083	0.297	0.144
MME	0.085	0.050	0.110	0.085	0.12	0.336	0.135
FS	0.090	0.083	0.094	0.085	0.081	0.244	0.138
$z = 0.36H$							
WT	0.053	0.059	0.035	0.028	0.054	0.142	0.048
MME	0.056	0.048	0.044	0.042	0.059	0.161	0.082
FS	0.098	0.096	0.074	0.068	0.056	0.182	0.142

[a] Local peak at the nose.
[b] Local peak at the tail.

3.2. Comparison across methodologies

The slipstream results from the three methodologies are directly compared in this section. Important characteristics of the time-average (raw and 1 s MA), standard deviation and peak (raw and 1 s MA) slipstream profiles are summarised in Table 2.

3.2.1. Time-average slipstream profiles

The time-averaged profiles (ensemble averages for the full-scale and moving-model results), both raw and with an equivalent 1 s moving-average (MA) are presented in Fig. 8 for the two measurement heights similar amongst the three methodologies. The 'standard slipstream profile': a local peak at the nose passing, increasing slipstream velocity along the sides due to thickening boundary layer, local peak at the tail passing followed by the largest peak in the near-wake, is visible in the mean profiles for each of the methodologies at both measurement heights ($z = 0.05\&0.36H$).

Immediately noticeable is the difference in length of the HSTs modelled, with the full-scale train having a $L/H = 50$, significantly larger than the $L/H = 16\&14$ of the moving-model and wind-tunnel models respectively. The presence of ambient wind in the full-scale field experiments is identified with a level of $\sqrt{u^2 + v^2} \approx 0.01u_t$ upstream of the nose, in spite of the run selections prioritising low ambient wind.

The local peak in slipstream at the nose is similar in magnitude ($\sqrt{u^2 + v^2} \approx 0.09u_t$) at $z = 0.05H$ for both the full-scale and moving-model, while the wind-tunnel exhibits a smaller peak of $\sqrt{u^2 + v^2} = 0.056u_t$. This difference is likely due to the proximity of the scaled wind-tunnel models nose to the front of the splitter plate, potentially influencing the pressure field around the nose. This is an experimental limitation that was deemed acceptable as the model was located to model the wake as best as possible, therefore having a short spacing between the model and splitter plate leading-edge plate. This reduced the development of the ground boundary layer which was a priority. At the larger heights, both the scaled results exhibit lower nose peaks than at full-scale, however there is no clear explanation for this difference.

Close inspection of the moving-model nose peaks identifies a double peak that is not apparent in the full-scale results. This is due to the forward facing probe arms used in the scaled experiments, which prohibit the measurement of reversed flow (accelerated flow around the trains nose) that is able to be measured in full-scale by the vertically mounted ultra-sonic anemometers.

The boundary layer development is significantly larger in the full-scale results than both the scaled results, at all measurement heights developing to $\sqrt{u^2 + v^2} \approx 0.05u_t$ with no clear difference between the full-scale results at different heights. This result is as expected as the full-scale operational train, although operating at a significantly larger

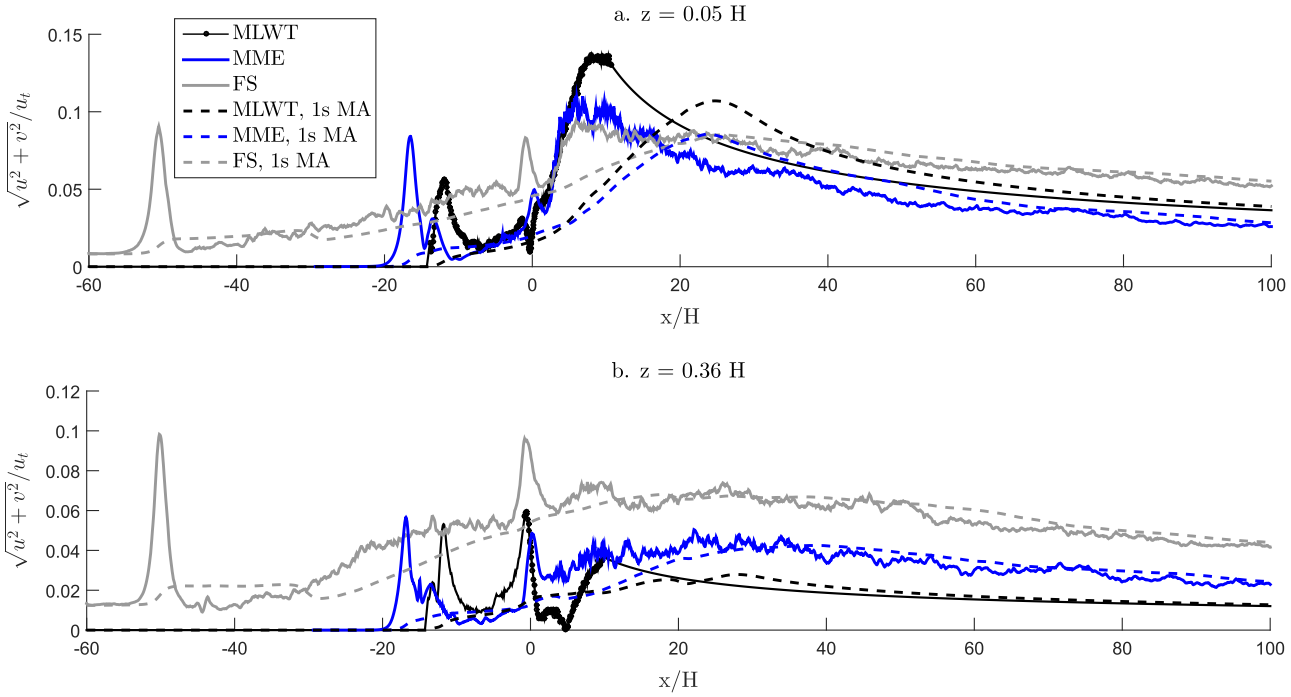

Fig. 8. Full-scale (FS), Moving-model experiment (MME), Monash Large Wind-tunnel (MLWT) measured time-average slipstream velocity, $sqrtu^2 + v^2$, at (a) z=0.05 (b) $0.36H$. Results are presented with (dashed line) and without (solid line) an equivalent 1 s moving-average.

Reynolds number, has more small scale geometry such as inter-carriage gaps, window seals and doors, as well as having a significantly larger relative length. The level of slipstream measured in the boundary layer is similar between the two scaled methodologies.

The magnitude and shape of the local peak in slipstream velocity at the tail is significantly different across the three methodologies. The local peak is preceded by a minor drop in the slipstream following the section of increasing slipstream caused by the thickening boundary layer. The moving-model and full-scale exhibit both a clear local peak. The relative magnitude above that of the level of slipstream developed to from the boundary layer is similar ($\sqrt{u^2+v^2} \approx 0.25u_t$ at $z = 0.05H$, $\sqrt{u^2+v^2} \approx 0.40u_t$ at $z = 0.36H$). However, the magnitude of the peak itself is significantly greater for the full-scale results. This is significant as the local tail peak is the largest slipstream velocity for the two higher measured positions, $z = 0.30\&0.36H$, although it is a sharp peak which is not visible in the respective 1 s moving-average profiles. The wind-tunnel results do show a tail peak at the higher measurement position ($z = 0.36H$). At the lower position ($z = 0.05H$) however, the small drop preceding the peak is more clearly defined and only a mere inflection point is visible where the other methodologies exhibit a clear local tail peak. This appears to occur due to the near-wake peak dominating the slipstream profile at this height.

The magnitudes of the near-wake peak at the lower height of $z = 0.05H$ are the most important as this is where the highest slipstream velocities occur, and where a full-scale HST is assessed for its slipstream. The near-wake peaks are similar in location at $x \approx 7H$ for all methodologies, however their magnitudes vary. The magnitudes are $\sqrt{u^2+v^2} = 0.094, 0.110\&0.136u_t$ at $z = 0.05H$ for the full-scale, moving-model and wind-tunnel profiles respectively. However, the corresponding 1 s moving-average profiles are much closer at these heights, with the moving-model and full-scale being the same ($\sqrt{u^2+v^2} = 0.85u_t$). At the higher measurement positions, the trend is reversed, and the full-scale near-wake peak in slipstream is larger than both the moving-model and wind-tunnel results. At all positions, the slipstream in the full-scale wake decays far slower than the moving-model slipstream.

The ideal nature of the scaled experiments, where no ambient wind exists, provides a possible explanation for the stronger near-wake peaks compared to full-scale at $z = 0.05H$ and a weaker peak at higher measurement positions. The presence of the ambient wind and atmospheric turbulence in full-scale may reduce the coherence of the turbulent structures that exist in the wake, most importantly a pair of streamwise vortices. This reduced coherence should result in a 'noisier' wake structure spreading out the induced flow within the core of the vortices outwards. The lower measurement height of $z = 0.05H$ is directly within the paths of these structures, whereas the higher measurement positions are on the upper, outer edge, and as such has lower slipstream velocity (Bell et al., 2016a). Consequently, any minor changes to the wake are more easily observed through higher measurement positions, as the dominant flow feature, the streamwise vortex is measured less directly, and such measurement positions are located in a region with high velocity gradients. This difference in coherence in the wake between full-scale and scaled wake also explains the slower decay rate of slipstream of the full-scale slipstream profile at all measurement heights.

The significantly larger Reynolds number of the full-scale wake is expected to further decrease the coherence of these turbulent structures, although their presence is still established through the peak and high variation in the near-wake of the full-scale results. The effect of the different boundary layers resulting from different train length's is investigated and discussed in Section 3.3.2.

The uncertainty and sensitivity of the moving-model ensemble average previously published by the authors (Bell et al., 2015) strengthens the comparison between the two scaled methods. The wind-tunnel magnitude of the near-wake peak of $\sqrt{u^2+v^2} = 0.135u_t$ at $z = 0.05H$ falls within the standard uncertainty of the moving-model ensemble calculated from 60 runs. An alternative explanation for the additional velocity in the near-wake peak of the wind-tunnel results could be attributed to the stationary floor and resulting boundary layer increasing the deficit in the freestream velocity and thus artificially increasing the measured slipstream velocity.

The overall agreement in ensemble average profiles suggests that both scaled methodologies represent and measure the flow around a high-speed train, however, in a cleaner, more ideal manner to that of full-scale. This difference is argued to be due to the reduced coherence

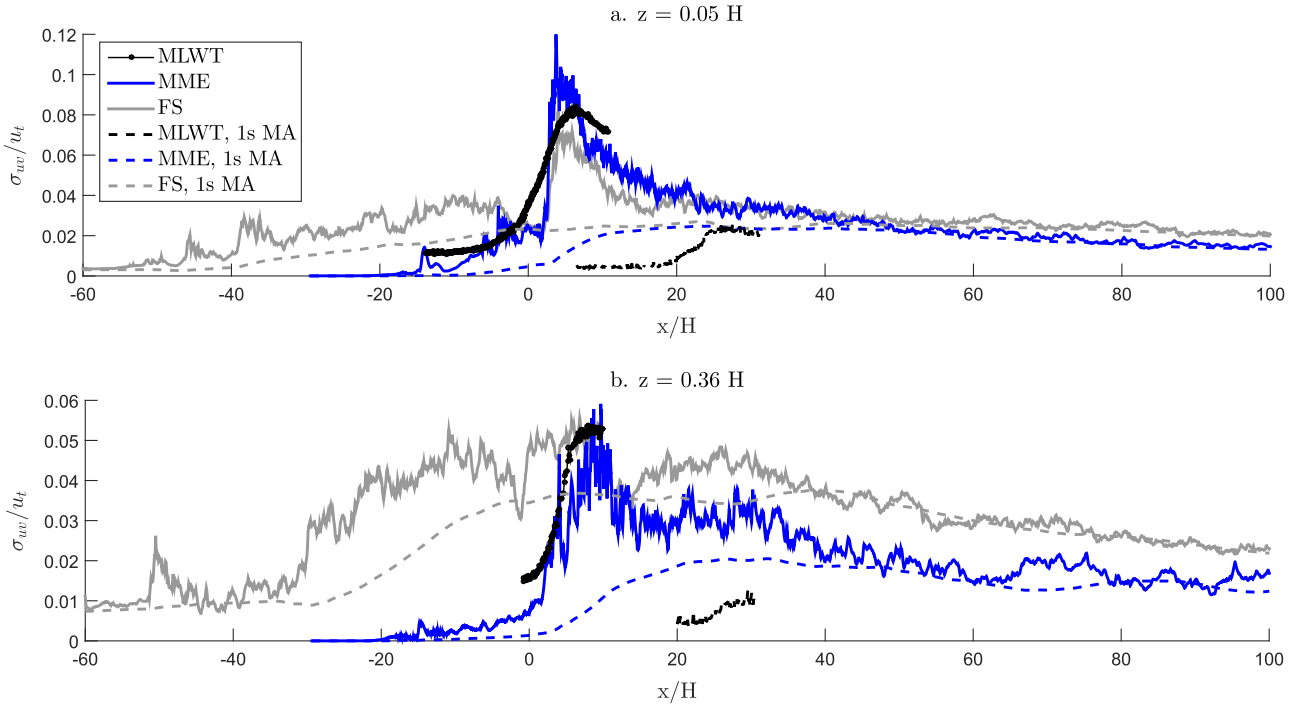

Fig. 9. Full-scale (FS), Moving-model experiment (MME), Monash Large Wind-tunnel (MLWT) standard deviation of slipstream velocity, σ_{uv}, at (a) z=0.05 (b) 0.36H. Results are presented with (dashed line) and without (solid line) an equivalent 1 s moving-average.

of the salient features in the full-scale wake resulting from ambient winds, atmospheric turbulence, and a significantly higher Reynolds number.

3.2.2. Standard deviation slipstream profiles

The standard deviation profiles of the slipstream velocity are presented in Fig. 9. In general, the standard deviation is low at the nose peak, illustrating its highly repeatable nature. This also occurs at the tail of the train, albeit to a lesser extent, suggesting some variation run-to-run of the tail peak. The near-wake experiences the highest deviation, with a peak standard deviation magnitude similar to the near-wake peak in the time-average. However, the standard deviation downstream of the peak decays much earlier in comparison to the time-average velocity profiles.

The peak in standard deviation in the near-wake compares well across all methodologies at $z = 0.05H$ for both the raw and equivalent 1 s moving-average profiles. The magnitude of the peaks of $\sigma_{uv} = 0.081$, 0.083&0.120 for the full-scale, wind-tunnel and moving-model are significantly greater at $z = 0.05H$ than the higher position, thus this position exhibits the largest mean and fluctuating slipstream velocity. The peak standard deviation at $z = 0.36H$ is also similar across the three methodologies, however the sharpness of the raw peak results in a significant difference in the peak of the equivalent 1 s moving-average standard deviation profiles, where the moving-model, and to a greater extent the wind-tunnel exhibits significantly lower standard deviation.

These differences in the standard deviation profiles at the higher position is likely due to greater sensitivity of these measurements to minor differences in the wake due to the measurement positions relative location to the streamwise vortices as discussed above.

3.2.3. Peak slipstream profiles

A representation of the largest peak slipstream velocity is presented in Fig. 10. The large magnitude of the peaks in the $\sqrt{u^2 + v^2} + 2\sigma_{uv}(x)$ profiles at up to $0.35u_t$ (105 km/h when $u_t = 300$ km/h) provide clear motivation for the investigation of the slipstream of HSTs.

The raw profiles represent the largest instantaneous slipstream velocity a stationary observer would experience at the measurement position. These compare relatively well across the methodologies at $z = 0.05H$. The scaled wind-tunnel and moving-model results compare well to each other, with near-wake peaks of $\sqrt{u^2 + v^2} + 2\sigma_{uv} = 0.30u_t$, slightly larger than the full-scale peak of $\sqrt{u^2 + v^2} + 2\sigma_{uv} = 0.25u_t$. The profiles of $\sqrt{u^2 + v^2} + 2\sigma_{uv}$ with a equivalent 1 s moving-average represent the peak gusts with a duration of 1 s or longer that a stationary observer would experience. The moving-average profiles of the three methodologies also compare well at $z = 0.05H$, with near-wake peaks of the similar magnitude ($[\sqrt{u^2 + v^2} + 2\sigma_{uv}]_{1sMA} \approx 0.14u_t$).

Similar to the standard deviation profiles, the raw profiles of $\sqrt{u^2 + v^2} + 2\sigma_{uv}$ at $z = 0.36H$ compare well, with both the scaled wind-tunnel and moving model near-wake peaks of $\sqrt{u^2 + v^2} + 2\sigma_{uv} = 0.14u_t$ at $z = 0.36H$ being similar to the $\sqrt{u^2 + v^2} + 2\sigma_{uv} = 0.17u_t$ of the full-scale peak. However, the moving-model and wind tunnel profiles with the equivalent 1 s moving-average applied exhibit significantly lower magnitude near-wake peaks (0.9&0.05u_t respectively) than full-scale (0.15u_t).

3.3. Sensitivity of slipstream results

In this section, the sensitivity of slipstream results to the ground boundary layer present in the wind-tunnel, train length and ambient wind is presented.

3.3.1. Wind tunnel ground boundary layer influence

The stationary floor present in the wind-tunnel methodology is an experimental limitation that is not easily overcome. The stationary floor results in a boundary layer that develops along the ground, which does not occur in full-scale HST operation. Boundary layer suction or a moving floor (rolling road) are difficult to apply and costly solutions, particularly in the case where the track and ballast shoulder ground configuration is modelled. Kwon et al. (2001) highlight the difficulties of applying such solutions to HST experiments, where the trains' long bodies means great care must be taken to apply suction at multiple slot locations, noting that their position could influence drag measurements.

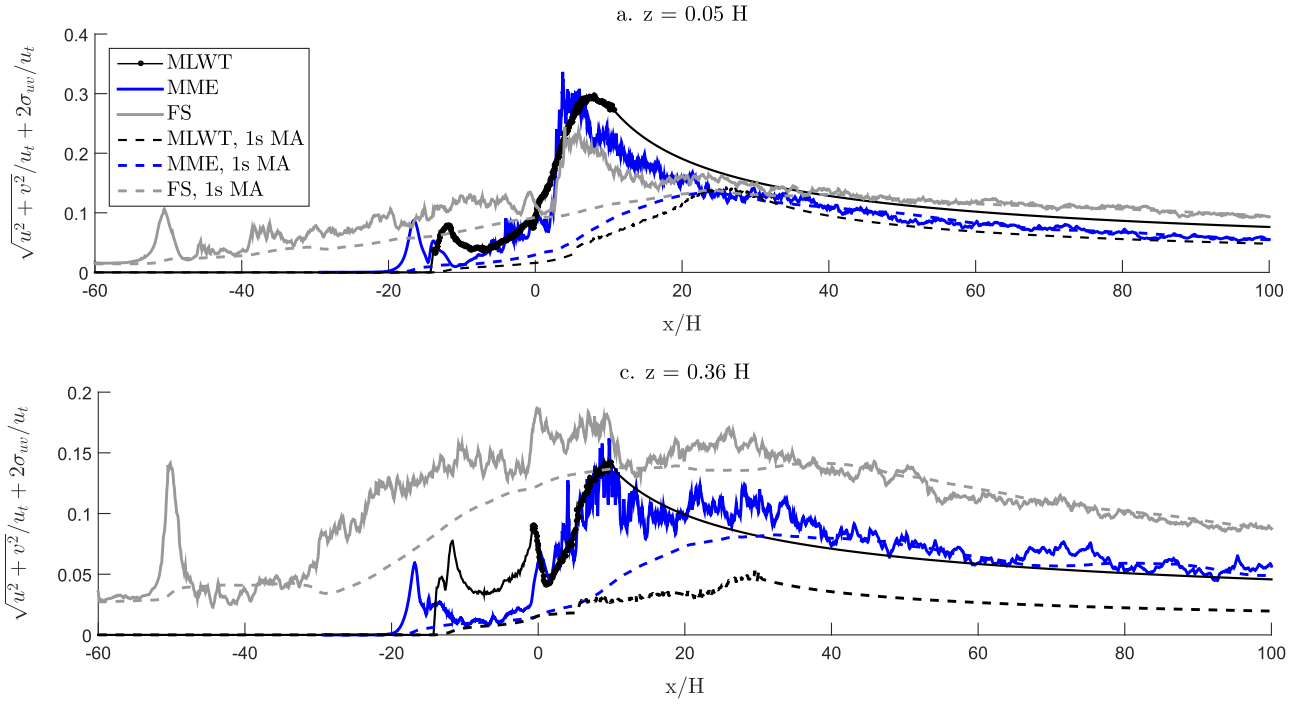

Fig. 10. Full-scale (FS), Moving-model experiment (MME), Monash Large Wind-tunnel (MLWT) 95% confidence interval of slipstream velocity, $\overline{uv} + 2\sigma_{uv}$, at (a) z=0.05 (b) $0.36H$. Results are presented with (dashed line) and without (solid line) an equivalent 1 s moving-average.

Due to the train-fixed frame-of-reference in the wind-tunnel experiment, the deficit in freestream velocity, u_∞, is considered the induced flow 'slipstream' in a ground-fixed frame-of-reference (Eq. (1)). The boundary layer developing over the stationary surface of the splitter plate in the wind-tunnel experiment is a deficit in the free-stream velocity, however, it is not the train's slipstream which is of interest. To understand the effects the stationary floor has on slip-stream results, slipstream measurements with and without the scale model present in the test-section are presented in Fig. 11.

As the height of the boundary layer is growing with increasing streamwise distance, the deficit in freestream velocity increases. This results in a perceived mean slipstream value of $\sqrt{u^2+v^2} = 0.075u_t$ at $x = 10H$ at the lower measurement position ($z = 0.05H$) in comparison to the $\sqrt{u^2+v^2} = 0.14u_t$ induced by the scaled-model. At the higher measurement position of $z = 0.36H$, the effects of the boundary layer are far less, reaching a maximum slipstream value of $\sqrt{u^2+v^2} = 0.020u_t$ at $x = 10H$. The standard deviation of the slip-stream velocity is similarly affected due to the turbulence within the boundary layer (Fig. 11b).

The presence of the scaled-model in the test-section influences the boundary layer on the ground. This is clear in Fig. 11a where the slipstream profiles with the model in the test-section are below that of the empty test-section. The strength of the wake of the HST dominates the area where slipstream is being measured, effectively washing away a significant portion of the boundary layer (Bell et al., 2016a). Thus, deficit in the freestream velocity from the boundary layer that occurs in the empty tunnel, and the flow from the HST model are not simply superimposed onto each other.

These results indicate that although the presence of the ground boundary layer is expected to have some effect on the slipstream results, this effect is not expected to be major, particularly in the vicinity of the streamwise vortices responsible for the near-wake peaks. The similarities in near-wake peak magnitudes and general slipstream profile characteristics between the three methodologies (where the moving-model and full-scale do not experience a ground boundary layer caused by a stationary floor) supports this proposition.

3.3.2. The effect of train length modelled

The key motivation for investigating the L/H is the concern that modelling a reduced L/H in the range 10-15, rather than full-scale of

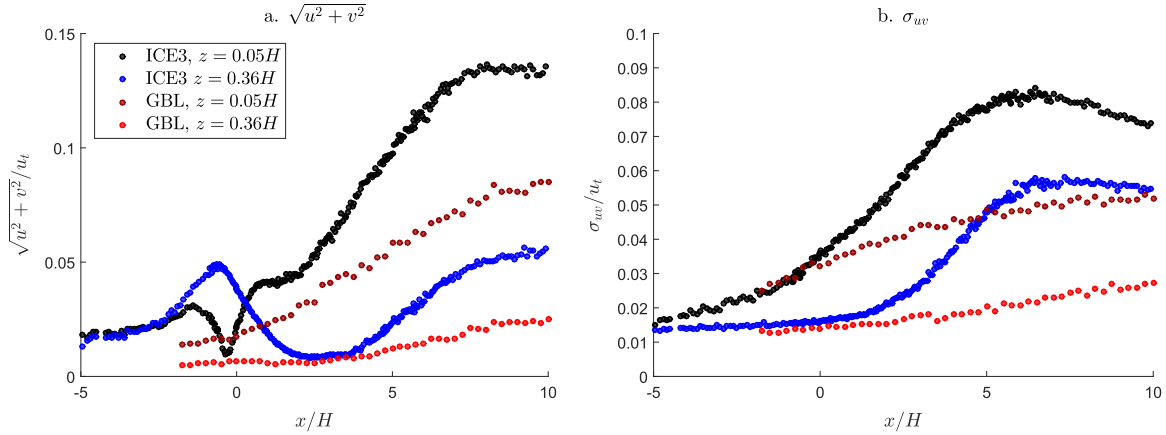

Fig. 11. Slipstream measured at z = 0.05, &0.36H with and without the scaled-model present in the test-section. (a) $\sqrt{u^2+v^2}$, (b) σ_{uv}.

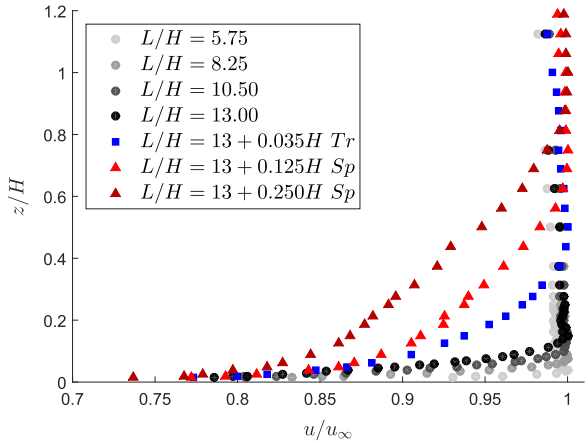

Fig. 12. Boundary layer velocity profiles, u/u_∞ for the different L/H wind-tunnel models, measured over the roof at $x = -2.5H$, $y = 0(W/2)$.

L/H=25–50, results in a different relative size boundary layer over the train, which reduces the similarity of the wake and resulting slipstream measurements.

The reduced length-to-height ratio in wind-tunnel experiments is necessary to allow as large a scale model as possible in the test section, in order to achieve high Reynolds numbers. This is also a limitation of moving-model experiments for similar practical reasons such as model weight, firing/braking mechanisms and track length. The high L/H of HSTs also presents a challenge numerically, as although technically they are not limited by physical space considerations, excessive computational resource requirements become an issue, with increased L/H coming at the cost of reduced Reynolds number and grid refinement. Although acknowledged in the literature (Weise et al., 2006), only recently has L/H been investigated by Muld et al. (2013); however, the effect of L/H has yet to be explicitly quantified.

The effect of L/H on slipstream was not able to be clearly identified in moving-model slipstream results previously published (Bell et al., 2015), where the length was changed from $L/H = 12 - 16$ and the Reynolds number was changed from 2.5–3.3 × 10^5. This is likely due to the insufficient range of L/H tested to influence a significant difference in the boundary layer over the different models.

Table 3
Boundary layer characteristics for different L/H.

L/H	δ/H	δ^*/H	θ/H
5.75	0.0280	0.0014	0.0013
8.25	0.0550	0.0051	0.0045
10.50	0.0850	0.0082	0.0071
13.00	0.1200	0.0110	0.0095
13 + 0.035H Tr	0.3200	0.0220	0.0200
13 + 0.125H Sp	0.5400	0.0360	0.0320
13 + 0.250H Sp	0.7800	0.0630	0.0550

The boundary layer profiles of the different wind-tunnel model configurations are presented in Fig. 12, the boundary layer thickness, δ, displacement thickness, δ^*, and momentum thickness, θ, for all cases are presented in Table 3.

The boundary layer velocity profiles progressively increase in thickness (Fig. 12) with increasing length (L/H = 5.75, 8, 25, 10.5, 13). However, each of the trips causes a large incremental increase in boundary layer size. These results establish that a large variation in the boundary layer ($\delta^*/H = 1.4 \times 10^{-3} - 6.3 \times 10^{-2}$) approaching the tail existed for the different scenarios, providing a good basis on which to assess the effect that the boundary layer has on the slipstream.

The boundary layer thicknesses achieved in the experiment are in the lower range of boundary layers measured on full-scale operational HSTs by Sterling et al. (2008) of $\delta^*/H = 5 \times 10^{-2} - 1.0 \times 10^{-1}$ and $\delta^*/H = 7.5 \times 10 - 2$ predicted by Pii et al. (2014) in full-scale, full-Reynolds number numerical simulations.

The mean slipstream profiles (Fig. 13), measured at $z = 0.05H$&$0.30H$ in the wind-tunnel, show that increased train length in general increases the level of slipstream. This is intuitive as a longer train with correspondingly thicker boundary layer is expected to induce a wider wake region. However, the near-wake peak in the $z = 0.05H$ profiles is largely insensitive to different L/H. This may be because the streamwise vortex causing this peak is not significantly influenced by upstream boundary layer thickness. In contrast, the slipstream upstream of where the streamwise vortex passes through the measurement point, and similarly at $z = 0.30H$ the larger boundary layer increases the overall slipstream. A thicker boundary layer affects the slipstream where the streamwise vortex is not directly measured: upstream, prior to the vortex moving outwards into the measurement position, and at the higher measurement position, $z = 0.30H$.

The increased slipstream velocity for the larger L/H at the higher measurement positions bring the magnitude of slipstream velocity closer to those observed in the full-scale experiments of $\sqrt{u^2 + v^2}/u_t \approx 0.7$ in the near-wake peak. Thus, the difference in between the full-scale and the scaled slipstream results could be due to the reduced L/H in the scaled experiments. However, the effect of the ambient wind and increased Reynolds number could also be causing the difference in slipstream results. These effects have not been able to be isolated or investigated fully in the wind-tunnel experiments.

The standard deviation profiles (Fig. 14) are consistent, in that the near-wake peak at $z = 0.05H$ is largely insensitive to L/H, yet upstream and at $z = 0.30H$, are both affected. Interestingly, the models with

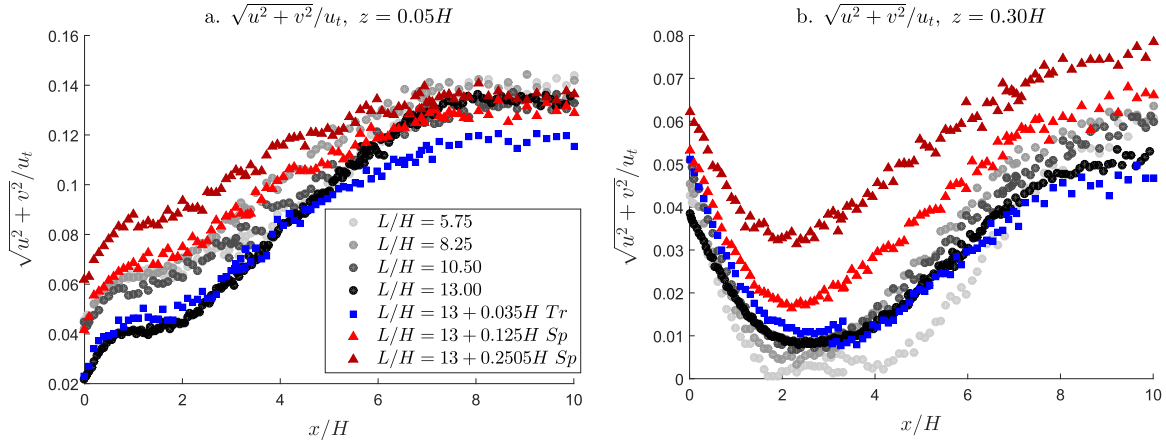

Fig. 13. Profiles of time-averaged slipstream velocity, $\sqrt{u^2 + v^2}$, for each of the L/H configurations of the wind-tunnel model measured at (a) $z = 0.05H$ and (b) $z = 0.30H$.

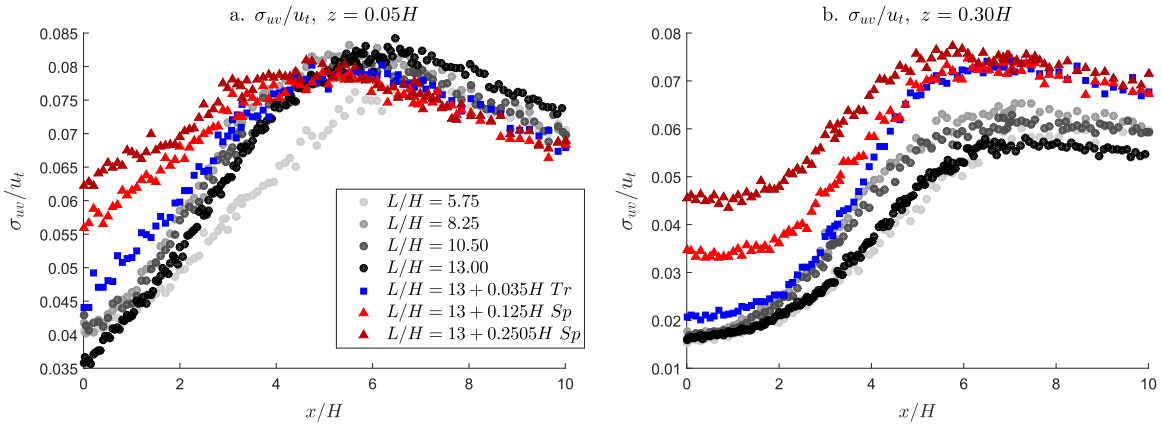

Fig. 14. Profiles of the standard deviation of slipstream velocity, σuv, for each of the L/H configurations of the wind-tunnel model measured at (a) $z = 0.05H$ and (b) $z = 0.30H$.

lower L/H have a slightly larger near-wake peak in standard deviation compared to those with larger L/H values.

Flow mapping in the wake for the same L/H range presented here, have previously been published by the authors (Bell et al., 2014). The primary findings were that the streamwise vortex that causes the near-wake slipstream peak is relatively insensitive to changing L/H. The larger L/H and corresponding increased surface boundary layer thickness do however increase the induced velocity above the streamwise vortices, which explains the higher sensitivity of slipstream results to L/H measured at higher positions. These results are broadly in line with the numerical results of Muld et al. (2013), as the primary features of the wake topology are consistent regardless of L/H.

5.75,8,25,10.5,13

The power spectral density (PSD) of the u component of velocity measured at $x = 1H$, $y = 1(W/2)$, $z = 0.2H$ for the different length configurations are presented in Fig. 15a. This was performed to investigate whether the unsteady wake, proposed to be the cause of the largest instantaneous slipstream velocities, is sensitive to L/H. All cases show a dominant frequency in the range $St = 0.16 - 0.24$. The trend of increasing L/H correlated with decreasing dominant frequency is clear. This trend has also been found in the numerical research by Muld et al. (2013). This is expected to be caused by the difference in effective width at the rear of the train caused by the surface boundary layer thickness dependence on train length, that is not taken into account in the length scale for non-dimensionalizing the frequency to form the Strouhal number.

To attempt to correct for this, the PSD of the u component of velocity signals were plotted against:

$$St^* = \frac{f\,(W + 2\delta^*)}{u_\infty} \tag{7}$$

in Fig. 15b. This changes the characteristic length used for non-dimensionalisation, originally the width of the model, to now include the additional widths of the surface boundary layer, where there is one on each side of the model. The boundary layer thickness over the roof was used as the boundary layers on the sides were not obtained for each L/H configuration. Of course, the thickness of the side boundary layers are expected to be larger than the those on the roof boundary.

This alternative calculation of the Strouhal number does improve the collapse the PSD profiles for each L/H case, with the range of the dominant peaks reducing, centred closer to St_W=0.2. However, they do not perfectly collapse, which indicates that the selection of the dominant frequency in the wake arises from more complicated physics.

Potentially, these L/H results indicate that boundary layer augmentation could be utilised to model a wake more representative of a larger L/H HST, specifically above the streamwise vortices. However, the effect of the reduced Reynolds number or presence of albeit small ambient wind have not been isolated and therefore are not ruled out as alternative causes of the difference in slipstream profiles at higher measurement positions.

Further insight could be gained from additional full-scale, track-side experiments, obtaining the boundary layer of a full L/H operational HST at multiple heights. This would additionally include the effects of finer geometry such as doors, inter-carriage gaps and realistic bogies for example. Such results would establish whether the different L/H, and the resulting difference in surface boundary layer was the cause of the poor representation of slipstream at high measurement positions in the scaled methodologies. Consequently, boundary layer augmentation as applied in the wind-tunnel experiment could be tuned to the full-scale boundary layer relative size and slipstream measurements could be taken.

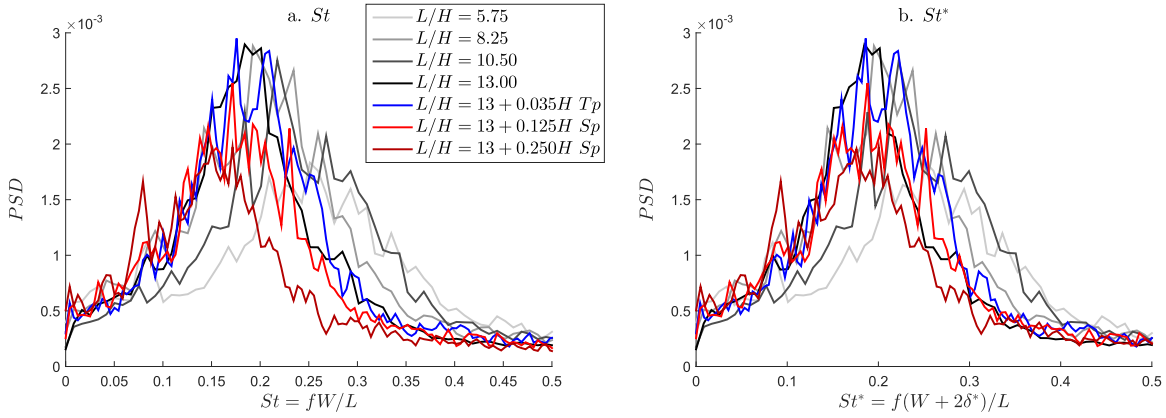

Fig. 15. Power spectral density of the u component of velocity at $x = 1H$, $y = 1(W/2)$, $z = 0.2H$ for different L/H configurations. (a) St, (b) St^* calculated using the displacement thickness added to the model width.

3.3.3. Full-scale ambient wind sensitivity

Ambient wind is the wind that exists in the local environment of the full-scale field experiment and is a difference between full-scale experiments to scaled moving-model or wind tunnel experiments. Thus, of the 294 full-scale ICE3 runs available for processing, 3 different run selection criteria have been applied and the results presented.

The first group of runs analysed were all 294 available. The second group were selected based on them passing the requirements to be included in slipstream assessment of a full-scale HST in the TSI regulations (ERA, 2008). To be included, the train speed must be within $u_t = \pm 10\% u_{t_{max}}$, where $u_{t_{max}}$ is the maximum operating speed of the HST, in this case 300 km/h (83.3 m/s). Additionally, runs are only accepted if the ambient wind, $u_{amb} < 2$ m/s, regardless of direction. This selection criteria resulted in 146 of the 294 total available runs being analysed as a group. The final selection criteria was based on the 60 runs with the lowest ambient wind, u_{amb}, on the condition that the train speed, $u_t > 78$ m/s. This resulted in a range of $u_{amb} = 0.1 - 0.95$ m/s $\approx 0.01 u_t$.

The presence of ambient wind and its inherent turbulence is identifiable in the difference between the ensemble mean, $\sqrt{u^2 + v^2}$, and standard deviation, σ_{uv}, respective profiles upstream of the nose for the three different run selection criteria (Fig. 16a and b respectively). As one would expect, the low ambient wind ensemble showed significantly lower wind and turbulence upstream than the TSI, followed by the all inclusive ensemble.

The local nose peak in $\sqrt{u^2 + v^2}$ was consistent for all three criteria regardless of the upstream difference. In contrast, the standard deviation at the local nose peak was affected by the ambient wind and turbulence present, increasing from the low wind case to TSI and then all runs. The presence of the ambient wind also appears to affect the developing boundary layer section of both the ensemble average and standard deviation profiles. However, the local tail peak in ensemble average velocity was consistent across the criteria, with similar levels of standard deviation.

The most important difference between the three profiles is the magnitude of the near-wake peak of the ensemble averages. The ensemble calculated from the 60 lowest ambient wind is larger than the other two criteria $\sqrt{u^2 + v^2} = 0.095$ compared to $\sqrt{u^2 + v^2} = 0.089$ and $\sqrt{u^2 + v^2} = 0.084$ for the TSI and all runs respectively. This is important as this run selection best represents the zero-ambient-wind condition modelled by the moving-model and wind-tunnel experiments. The individual runs and ensembles calculated from these 60 runs with lowest ambient winds are the results that are compared to the scaled experimental results.

4. Gust results

Gust analysis is performed to calculate the 'maximum airspeed' of a HST's slipstream which must not exceed a 'maximum permissible airspeed' in order to operate (ERA, 2008; CEN, 2009). Similar analysis is performed in the field of wind engineering to predict the effects wind gusts have on structural loading. The maximum airspeed ($uv_{2\sigma_{uv}}$) is the sum of the mean and two times the standard deviation of a data set that is comprised of the peaks of each individual full-scale runs with a 1 second moving average. It is therefore necessary for a scaled methodology to be able to predict the maximum airspeed and determine if it is below the regulated maximum permissible airspeed.

4.1. Wind-tunnel gust analysis methodology

Gust analysis can not be performed to the scaled wind-tunnel slipstream point-wise measurements in the same manner as for the scaled moving-model and full scale measurements. This is due to the measurements being obtained in a point-wise manner performed in the train-fixed (TF) frame-of-reference for wind-tunnel measurements,

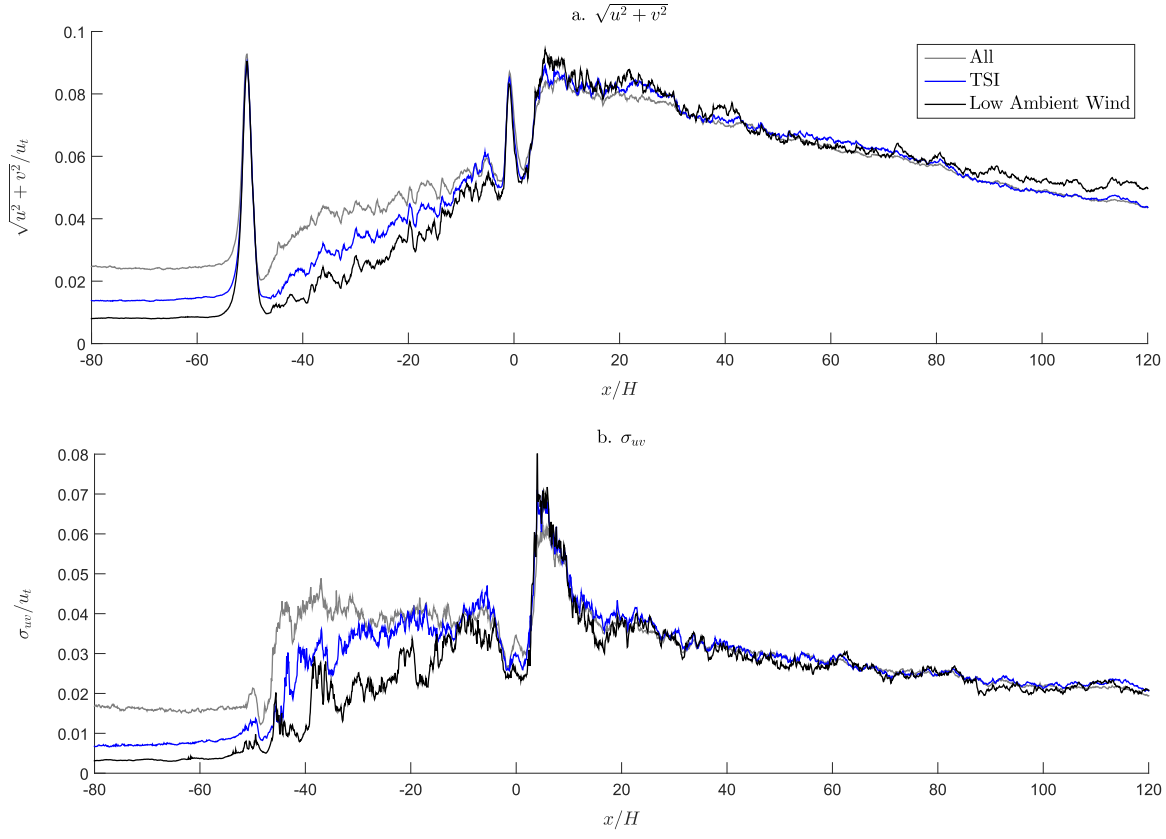

Fig. 16. Full-scale (FS) measured ensemble results of slipstream velocity for three run selection criteria: All measured runs, runs meeting TSI assessment criteria, and the 60 runs with lowest ambient wind. Ensemble mean (a) $\sqrt{u^2 + v^2}$, and (b) ensemble standard deviation, σ_{uv} at $z = 0.05H$.

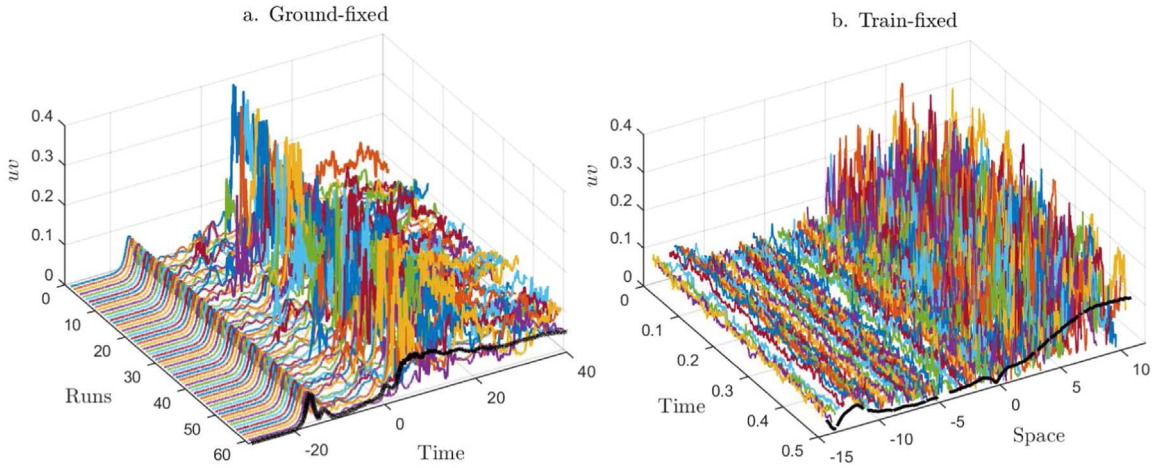

Fig. 17. The individual runs and ensemble average obtainable in (a) the ground-fixed (GF) frame-of-reference such from a moving model and full-scale field experiments, and (b) the point-wise time-series and streamwise time-averaged profiles obtainable in the train-fixed (TF) frame-of-reference from a wind-tunnel experiment.

whereas the moving-model and full-scale measurements are obtained in the ground-fixed (GF) frame-of-reference. The principal difficulty in applying gust analysis to TF type data is that no 'individual runs' exist for peaks to be determined from and then further processed to calculate a 'maximum airspeed'. Specifically, the difference in spatial and temporal correlation between the two data types is illustrated in Fig. 17.

Measurement obtained in GF frame-of-reference (Fig. 17a) are correlated in time, relative to the train's movement past the measurement equipment. This time can be converted to distance, relative to the train's tail, utilising the train's travelling velocity. However, each individual run, and corresponding peak is not correlated to any other.

In contrast, measurements obtained in the TF frame-of-reference (Fig. 17b) are correlated in time at each point in space measured (a time signal is obtained), but each measurement point is not correlated to another, as each was measured by a single probe, at different points in time.

The average and standard deviation profiles measured in the wind-tunnel are statistically equivalent to the ensemble average and standard deviation profiles, provided enough individual runs are measured. An equivalent moving-average is simply applied to the average profile measured in the wind-tunnel. However, the GF standard deviation profile is calculated from the standard deviation across the ensemble of individual runs with a moving-average applied. For the wind-tunnel TF measurements, the equivalent processing is applying a scaled 1 s moving-average to each individual time-series measured at each point in space in the streamwise direction. The $\overline{uv}_{2\sigma_{uv}}(x)_{1s\ MA}$ profile in the TF frame-of-reference is then a summation of the average and standard deviation profiles in spite of the 1 s moving average applied in different ways.

The moving-model and full-scale results below show that the maximum of the $\overline{uv}_{2\sigma_{uv}}(x)_{1s\ MA}$ profile is similar to the maximum airspeed ($uv_{2\sigma_{GF}}$) calculated from individual runs, and across those GF results, consistently less by a small margin (Figs. 19 and 20). The maximum airspeed ($uv_{2\sigma_{GF}}$) in the GF measurements of both moving-model and full-scale is on average 1.08 times larger than the maximum of $\overline{uv}_{2\sigma_{uv}}(x)_{1s\ MA}$ profile. The generality of 1.08 as a factor to other train geometries, has not been established, an investigation of a variety of different geometries would be required to do so. This does however provide a simple method to estimate the maximum airspeed of an ICE3 in the TF frame-of-reference from the $\overline{uv}_{2\sigma_{uv}}(x)_{1s\ MA}$ profile:

$$uv_{2\sigma_{uv}TF} \approx 1.08 \times \max[\overline{uv}_{1s\ MA}(x) + 2\sigma_{uv1s\ MA}(x)]. \quad (8)$$

Alternatively, the temporal correlation and probability distribution of each point-wise measurement can be utilized to create conditional probability distributions and subsequently construct 'individual runs' from the train-fixed frame-of-reference wind-tunnel data. The auto-correlation of each signal provides insight into how correlated a measurement is to other measurements downstream.

First, the Taylor's hypothesis, linking space and time using a convection velocity, is utilised to estimate how correlated velocity at one point is to all the points in space measured downstream.

The level of correlation is quantified by the correlation coefficient, ρ, over the range −1 to 1. The magnitude of correlation is used to create a conditional probability distribution by limiting the range of the entire probability distribution which has a range of $0 < Pr < 1$, at each position with Pr=0.5 being the median. Because the level of correlation has a magnitude less than 1 at any level of lag, there remains some uncertainty or range that the conditional probability can be. The upper and lower limits of this range is calculated by:

$$Pr_i = (A + B \times Pr_{i-j}) \pm C \quad (9)$$

where A and B are dependant on the sign of the correlation, regardless of the magnitude:

$$\rho_{i,i-j} > 0, \quad A = 0, \ B = 1, \quad (10)$$

$$\rho_{i,i-j} < 0, \quad A = 1, \ B = -1, \quad (11)$$

$$\rho_{i,i-j} = 0, \quad A = 0.5, \ B = 0. \quad (12)$$

The range of estimated probability is provided by C, which considers the magnitude of the correlation coefficient.

$$C = \frac{1 - |\rho_{i,i-j}|}{2} \quad (13)$$

For example, if $\rho_{i,i-j} = 0.8$ and $Pr_{i-1} = 0.7$, then $A = 0$, $B = 1$, $C = 0.1$ and $0.6 < Pr_i < 0.8$.

In contrast, if $\rho_{i,i+1} = -0.8$ (negative correlation) and $Pr_{i-1} = 0.7$ then $A = 1$, $B = -1$, $C = 0.1$ and $0.2 < Pr_i < 0.4$.

The probability can be estimated from the autocorrelation with a longer lag and the probability of further and further positions upstream.

Thus, at each position i, a conditional probability range, Pr_i, is calculated based on the upstream probability (Pr_{i-j}) and the correlation level $\rho_{i,j}$ at each upstream position (j). The average, $\overline{Pr_i}$ conditional probability range was calculated at each point, and the Matlab function *rand* was used to randomly select a Pr_i within this range. Thus, from a starting point, each downstream position is estimated incrementally using this process, with the history of velocity at previous positions being considered.

This process was performed 50 times at each starting point. There were 100 starting points, at $x = 0H$ which were $Pr_i = 0 - 1$ in 0.01

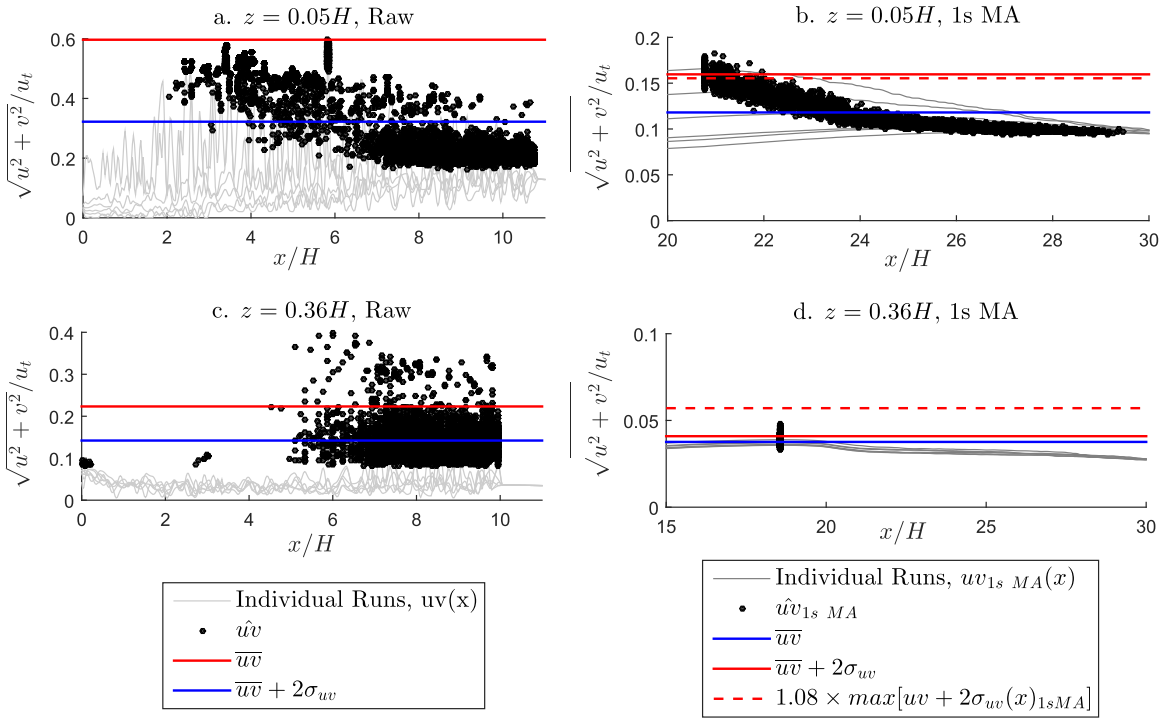

Fig. 18. Peak values from individual runs constructed using the wind-tunnel data measured at $z = 0.05\&0.36H$. Mean, $\overline{uv}$, and $\overline{uv} + 2\sigma_{uv}$ of the peaks are denoted as blue and red lines respectively. Approximate $\overline{uv} + 2\sigma_{uv}$ calculated by Eq. (8) denoted as dashed red line.

increments. This resulted in 5000 individual runs constructed from the wind-tunnel data.

The mean profile upstream of the starting point was appended to the constructed runs, as well as the basic decay relationship to the end $x > 11H$ as outlined in Section 3.1. This process provided a longer profile for the $x = 20.8H$ spatial moving-average to be applied to.

The constructed individual runs were analysed raw, with a $0.08H$ spatial moving-average applied to them prior to the peaks being determined. This average was also added to the 'raw' moving model individual runs. This process converts these results to the same spatial resolution as the full-scale results, which had a scale-relative lower spatial sampling frequency. An equivalent to a 1 s moving-average was also applied (corresponding to $x = 20.8H$ in space), where the corresponding peaks are located further downstream due to the lag of the moving-average.

4.2. Comparison of gust results across the methodologies

4.2.1. Peak values

The peak velocities from each of the constructed individual runs from wind-tunnel data, individual runs measured in the moving-model and full-scale experiments are presented in Figs. 18, 19 and 20 respectively. Instantaneous, 'raw', and with an equivalent 1 s moving-average peak velocities are presented.

The results at $z = 0.05H$ are qualitatively similar to those of the moving-model and full-scale experiments, with clusters of peaks in the wake for both the raw and 1 s moving-average constructed runs. However, at the higher measurement position $z = 0.36H$, the raw peaks are not as widely distributed in the wake. This is explained by the reduced coherence of the streamwise vortices at higher positions, that are expected to cause the peak velocities.

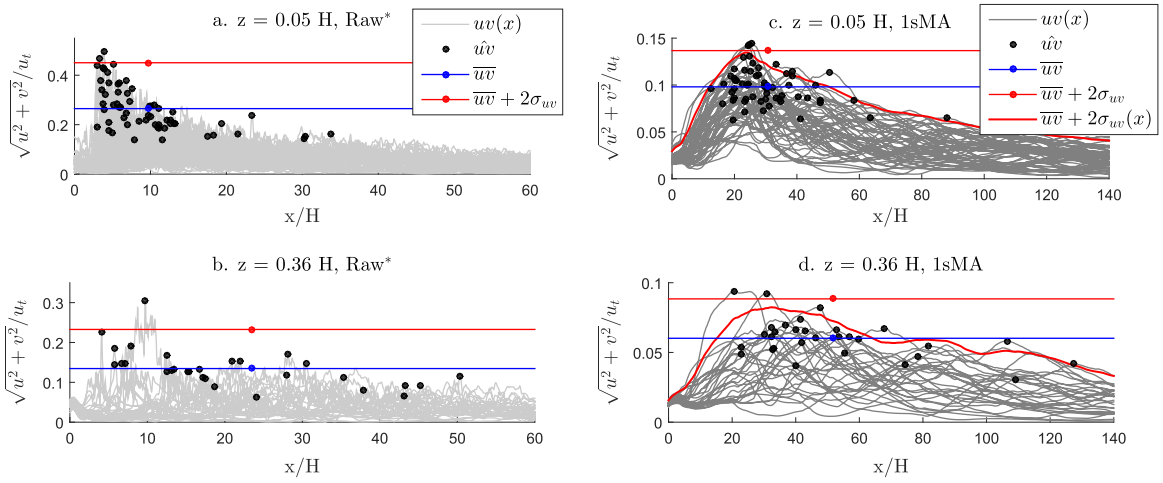

Fig. 19. Peak velocities of each individual runs; (a,b) raw and (c,d) with a 1 s equivalent moving-average measured in the moving-model experiment at (a,c) $z = 0.05H$ and (b,d) $z = 0.36H$. Mean, $\overline{uv}$, and $\overline{uv} + 2\sigma_{uv}$ of the peaks are denoted as blue and red lines respectively. (For interpretation of the references to color in this figure caption, the reader is referred to the web version of this paper.)

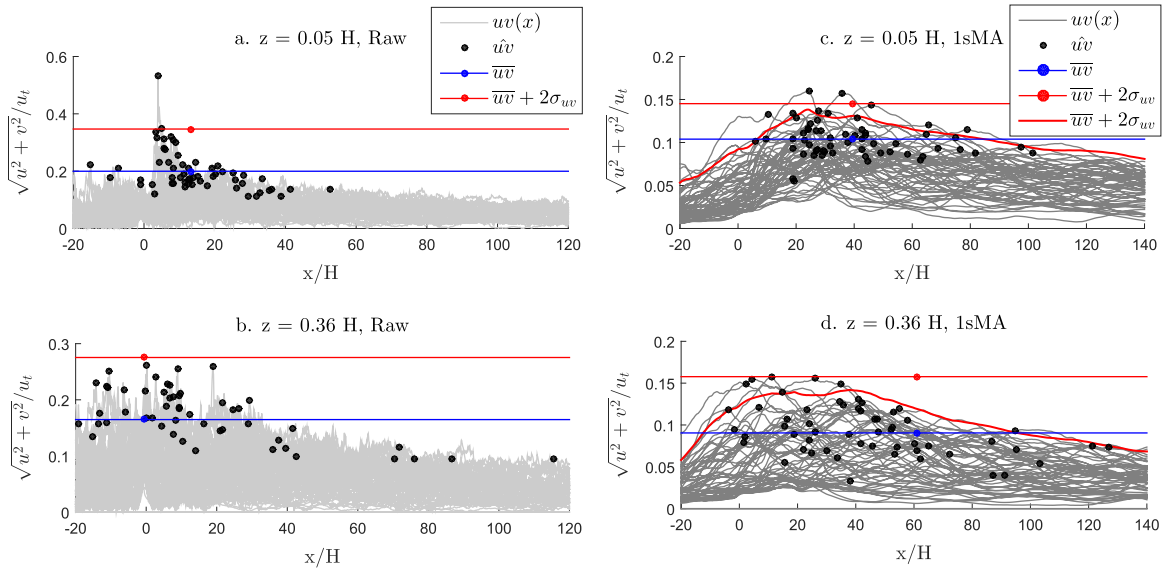

Fig. 20. Peak velocities of each individual run;, (a,b,c) raw and (d,e,f) with a 1 s equivalent moving-average measured in the full-scale experiment at $z = 0.05$, 0.30& $z = 0.36H$. Mean, $\overline{uv}$, and $\overline{uv} + 2\sigma_{uv}$ of the peaks are denoted as blue and red lines respectively. (For interpretation of the references to color in this figure caption, the reader is referred to the web version of this paper.)

Significant differences in the peak magnitudes and location in the wake remain in spite of the large moving-average applied. Distinct differences are also visible in the respective individual runs. These results indicate that large-scale turbulent structures, whose effects are not smoothed out by the moving-average, are responsible for the different peaks and individual runs.

The wind-tunnel peaks of the 1 s moving-averaged constructed runs all occur at the same position in the wake. This occurred as the local tail peak was the most dominant peak after the moving-average was applied and resulted in all peaks occurring at this position, with the wake velocity contributing to the difference in magnitude.

There are only minor differences in the magnitudes and locations of the peaks between the moving-model and full-scale results. The full-scale peaks appear to be more widely distributed in the wake. Additionally, a number of full-scale peaks occur upstream of the tail, which did not occur in the moving-model results. Both differences can be explained by the reduced coherence of the full-scale wake, due to the larger Reynolds number and presence of ambient wind. Alternatively, the peaks could be caused by the larger level of turbulence resulting from a larger L/H of the full-scale HST.

The $uv_{2\sigma} = 0.159u_t$ calculated from the constructed wind-tunnel runs at $z = 0.05H$ is in the range estimated (Eq. (8)) from the maxima of the sum of the ensemble average and standard deviation profiles, $uv_{2\sigma} = 0.155u_t$. However, at the higher measurement positions, the constructed runs exhibit significantly reduced fluctuation which results in a significantly lower predicted $uv_{2\sigma}$ compared to the expected $uv_{2\sigma}$ based on the ensemble and standard deviation profiles.

4.2.2. Statistical analysis of peak values

The distribution of the velocity magnitude and location in the wake of the peaks from the three methodologies are presented in Fig. 21, with the corresponding statistics provided in Table 4.

Comparison of the peaks observed in the scaled results to the full-scale results is similar to the comparison of the slipstream profiles presented above. The comparison is stronger at $z = 0.05H$, particularly for velocity magnitude of the raw peaks with similar low levels of skewness (0.41–0.99) and kurtosis (2.7–3.5).

Normally distributed peaks would exhibit skewness and kurtosis of 0 and 3 respectively. The velocity magnitude of the peaks are not normally distributed. Thus, the 'maximum airspeed', as the summation of the mean plus two times the standard does not necessarily represent the 95% confidence interval. As this relationship of 2 standard deviations to 95% confidence interval assumes a Normal distribution. The use of mean plus 2 standard deviations in estimating the 95% confidence interval does however, maintain a desirable simplicity for the value, which in itself is an somewhat arbitrary level of confidence.

The location of the peaks in the wake is similar for the moving-model and full-scale, however, the wind-tunnel peaks only occur within the measured region $x = 0 - 11H$ where runs were constructed. The limited length of the wake measured in the wind-tunnel is also the expected cause of the reduced width of distribution at the higher measurement position. Further, the individual run construction method does not appear as successful in constructing realistic runs at these higher positions.

The peaks from scaled methodologies at the higher positions were lower than those of the full-scale results, exhibiting both lower means and standard deviations of the peaks. These results again are similar to the trends identified in the slipstream profiles and are argued to be caused by the larger Reynolds number flow and ambient wind reducing the coherence of the full-scale wake, and additionally the thicker L/H of the full-scale train contributing turbulence higher in the wake due to the larger surface boundary layer.

4.2.3. Maximum airspeeds

The 'maximum airspeeds', $\overline{uv}2\sigma_{uv}$, calculated from the peaks of runs with an equivalent 1 s moving-average applied, which must be below the 'maximum permissible airspeed' specified by the TSI regulations for a HST to operate (ERA, 2008) are highlighted in Table 4 in bold. These values are also presented graphically in Fig. 22. The uncertainty of this value is $\approx \pm 0.005$ for the moving-model and full-scale results, based on the number of runs processed, and magnitude of the mean and standard deviation of the peaks.

Similarly to the comparison of the average slipstream profiles of the three methodologies, the results compare relatively well (moving-model −5.5%, wind-tunnel +9.6% compared to full-scale) at the lower measurement position of $z = 0.05H$ and relatively poorly at the higher positions of z=0.30 and $z = 0.36H$ (moving-model −44.3%, wind-tunnel −91.1% compared to full-scale). This is expected to be due to the reasons discussed above.

The range of maximum airspeeds of a number of other HSTs measured by Baker et al. (2012b), presumably due to the different geometries, put the magnitude of the differences between the full-scale

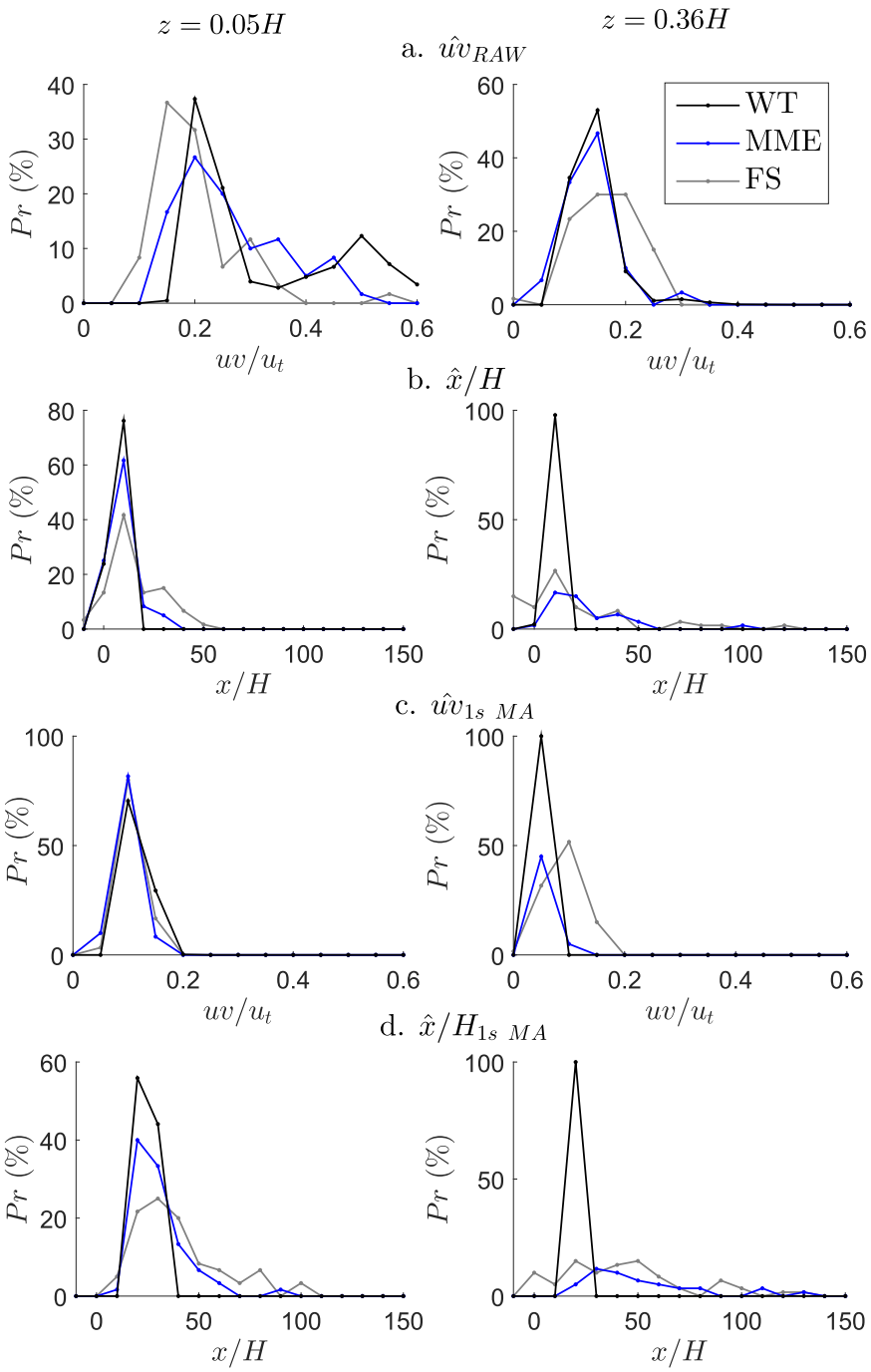

Fig. 21. Probability distribution of velocity magnitude and location of peak values at $z = 0.05$, &$0.36H$ for the three experimental methodologies: Monash Large Wind Tunnel (MLWT), Moving-model Experiment (MME), and Full-Scale (FS). Peaks from both 'raw' and with an equivalent 1 s moving-average applied to individual runs.

maximum airspeed and the scaled methodologies predicted maximum airspeed into perspective.

In full-scale measurements by Baker et al. (2012b) at the height of $z = 0.05H$, a variety of different HST geometries: S-100, S-102, S-120, S-130, have maximum airspeeds of 0.191, 0.174, 0.213, and $0.251u_t$. This corresponds to up to 70% difference of the maximum airspeed value of the ICE3. This range is large relative to the differences predicted by the scale models (5–10%) indicating both methodologies are suitable for identifying trends due to different parameters like geometry.

The implications of these results are that firstly wind-tunnel data has the potential to be used to construct individual runs, to which gust analysis can be performed. However, the method presented requires improvement, as it does not construct representative runs at the higher measurement positions well. Further, the reduced length of the wake measured limits the spatial range of gusts able to be measured.

The moving-model methodology enables direct gust analysis to be performed and consequently the results compare better to the full-scale results. However, as there are still differences in the slipstream profiles for both scaled methodologies, the respective gust results must also contain differences that need to be accounted for and improved prior to confidently using gust results for assessing the slipstream risk of HSTs using scaled methodologies.

In-spite of the full-scale ensemble average having a significantly lower magnitude in the wake at the higher measurement position ($z = 0.36H$), the large standard deviation results in a maximum air-

Table 4
Gust results from each methodology.

Height	$z = 0.05H$			$z = 0.36H$		
Method	WT	MME	FS	WT	MME	FS
a. uv						
$\overline{uv}$	0.322	0.265	0.199	0.142	0.135	0.165
σ_{uv}	0.137	0.093	0.073	0.041	0.049	0.055
$\overline{uv}2\sigma_{uv}$	0.597	0.451	0.347	0.223	0.233	0.275
Sk	0.75	0.72	1.93	2.22	1.37	−0.31
Kt	2.00	2.59	8.31	11.18	6.03	2.79
b. x						
$\overline{x}$	7.45	9.69	13.41	8.31	30.68	−0.71
σ_x	2.54	6.87	14.4	1.61	12.73	77.41
Sk	−0.45	1.79	0.08	−3.27	2.10	−5.42
Kt	1.81	6.1	3.54	18.15	8.60	38.52
c. $uv_{1s\ MA}$						
$\overline{uv}$	0.118	0.098	0.104	0.037	0.060	0.091
σ_{uv}	0.021	0.019	0.021	0.0016	0.014	0.034
$\overline{uv}2\sigma_{uv}$	**0.159**	**0.137**	**0.145**	**0.041**	**0.088**	**0.158**
Sk	0.99	0.41	0.46	0.83	0.43	−0.023
Kt	2.72	2.86	3.56	5.00	3.51	40.52
d. $x_{1s\ MA}$						
$\overline{x}$	24.49	23.54	39.64	18.57	51.69	61.17
σ_x	2.28	19.24	21.18	0	26.68	209.71
Sk	−0.09	2.02	1.01	1	1.30	5.28
Kt	1.78	8.83	3.57	1	4.05	40.52

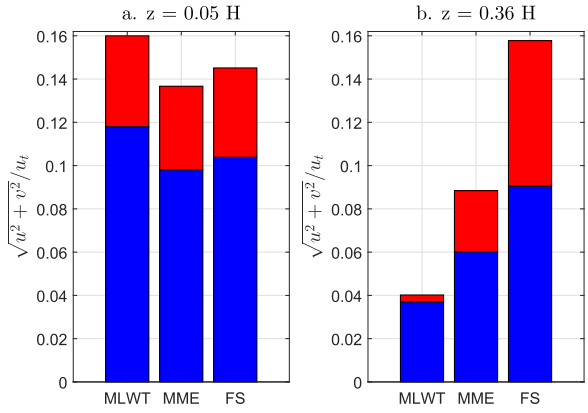

Fig. 22. The 'maximum airspeed' calculated at $z = 0.05H$ and $z = 0.36H$, for the three experimental methodologies: Monash Large Wind Tunnel (MLWT), Moving-model Experiment (MME), and Full-Scale (FS). The contribution of the mean and 2σ are indicated by blue and red respectively. (For interpretation of the references to color in this figure caption, the reader is referred to the web version of this paper.)

speed that marginally increases with measurement height. However, in full-scale this position corresponds to 2.6 m above the ground which is higher than a typical human who would be at risk standing track-side.

The contribution that both the mean and standard deviation make to the maximum airspeed (Fig. 22) presents a difficulty with using it as a comparative value for assessing the accuracy of the scaled methodologies. Potentially, different mean values combined with different standard deviations can provide the same value.

5. Conclusions

The accuracy of a 1/10th-scaled wind-tunnel methodology of measuring slipstream was assessed through comparison to scaled moving-model and full-scale results of the same ICE3 HST geometry.

The slipstream profile results showed relatively strong comparison at the lower measurement position of $z = 0.05H$: $\sqrt{u^2 + v^2} = 0.110\&0.133u_t$ for the wind tunnel and full-scale near-wake peak velocities respectively. This height is important as it is where the slipstream velocities are highest and currently assessed and regulated (ERA, 2008; CEN, 2009). Thus, there is greater priority to predict slipstream at this position accurately.

Differences between the three methodologies in the average slipstream profile and levels of standard deviation were observed at the higher measurement position ($z = 0.36H$). The expected cause for the differences between the full-scale and scaled methodologies is the reduced coherence of streamwise vortices due to presence of ambient wind, atmospheric turbulence and significantly larger Reynolds number in full-scale experiments. The measurements at the higher positions were more sensitive to minor changes in the wake due to their location on the edge of the streamwise vortices, rather than directly in the core at $z = 0.05H$.

The presence of a ground boundary layer developing over the stationary floor does affect slipstream measurements performed in the wind-tunnel with an empty test-section. However, the wake of the HST, responsible for the peak slipstream velocities, appears to dominate the measurements. The strong comparison of the wind-tunnel results to the moving-model and full-scale supports this proposition.

The wind-tunnel slipstream results indicated that the near-wake peak at the low measurement height ($z = 0.05H$) was insensitive to L/H. Prior to the near-wake peak, and at the higher measurement position ($z = 0.36H$), the slipstream measured was higher for large L/H, as would typically be expected due to the increased boundary layer and resulting thicker shear layers feeding into the wake. This results in the slipstream profiles exhibiting a near-wake peak at a much more similar magnitude to that of full-scale. These results highlight the potential for the application boundary layer augmentation to reduced L/H models to improve the accuracy of slipstream measurements. The exact methodology however, for instance the size of the spikes and resulting velocity profile, would greatly benefit from further insight into the surface boundary layer of an operational, full-scale HST.

Similarly to the slipstream profiles, the scaled methodologies gust analysis results compare relatively well at the lower measurement position ($z = 0.05H$), but poorer at higher measurement position to full-scale gust results. This is again expected to be due to the location of the measurement position relative to the core of the streamwise vortices proposed to cause the maxima.

The moving-model gust results were more similar to full-scale than the wind-tunnel results, in terms of the average, distribution and resulting estimation of the 'maximum airspeed' of which the slipstream risk of a HST is assessed and regulated. This is due to the restricted distance behind the HST model that can be measured in the wind-tunnel due to test-section size limits, as well as the inability for individual runs to be processed to directly perform gust analysis in the same frame-of-reference as full-scale.

A method for constructing individual runs from the point-wise wind-tunnel data was applied, utilizing the auto-correlation to create conditional probability distributions. This method represented individual runs at the lower measurement positions reasonably, but was unable to construct representative individual runs at the higher measurement positions.

From these results, the scaled methodologies investigated are both suitable for determining the slipstream risk of a HST, albeit in different ways. A wind-tunnel methodology is more suited to investigate a HST in the early design stage, taking 'relative' slipstream measurements. The ICE3 slipstream results could be used as a baseline case to compare the slipstream results of different prototype HSTs. These relative slipstream results, instead of absolute, would provide an indication of the full-scale operational slipstream risk of a HST when using the full-scale ICE3 results as an additional benchmark. Here, the benefits of the large data-set of full-scale runs measured of the ICE3 are realized. In such a method, the uncertainty from the stationary floor

and a complex run construction technique are reduced as they are constant for all cases investigated. Further, the time to measure the slipstream profile, with the scaled methodologies as described, is faster in wind-tunnels. This efficiency could be employed to test incremental geometric features or active flow control parameters (e.g. actuation frequency) whilst also measuring drag, cross-wind stability, and head-pressure pulse, which are also important aerodynamic characteristics of HSTs.

The moving-model methodology could be best utilized at a later stage in the design phase, where high confidence in gust analysis is required. However, the differences in results at higher measurement positions need to be established and if possible reduced. This requires further investigation into the effect of Reynolds number on the coherence of the wake and the effect of low levels of ambient wind, the latter of which can be feasibly investigated and modelled in moving-model experiments.

Acknowledgements

The Faculty of Engineering, Monash University is acknowledged for the Engineering Research Living Allowance stipend scholarship for J.R. Bell. The DIN Standards Railway Committee (FSF) is acknowledge for the providing the ICE3 geometry.

References

Baker, C., 2012. Wp5-d5.4 output document -recommendations for tsi revisions. AeroTRAIN Project Publication D6.3(1), A.5.1.

Baker, C., Quinn, A., Sima, M., Hoefener, L., Licciardello, R., 2012a. Full scale measurement and analysis of train slipstreams and wakes: Part 1 ensemble averages. Proc. Inst. Mech. Eng. Part F: J. Rail Rapid Transp..

Baker, C., Quinn, A., Sima, M., Hoefener, L., Licciardello, R., 2012b. Full scale measurement and analysis of train slipstreams and wakes: Part 2 gust analysis. Proc. Inst. Mech. Eng. Part F: J. Rail Rapid Transp..

Baker, C.J., 2001. Flow and dispersion in ground vehicle wakes. J. Fluids Struct. 15, 1031–1060.

Baker, C.J., 2010. The flow around high speed trains. J. Wind Eng. Ind. Aerodyn. 98, 277–298.

Bearman, P.W., Beer, D.D., Hamidy, E., Harvey, J.K., 1988. The effect of a moving floor on wind-tunnel simulation of road vehicles. SAE Technical Paper No. 880245.

Bell, J.R., Burton, D., Thompson, M.C., Herbst, A.H., Sheridan, J., 2014. Wind tunnel analysis of the slipstream and wake of a high-speed train. J. Wind Eng. Ind. Aerodyn. 134, 122–138.

Bell, J.R., Burton, D., Thompson, M.C., Herbst, A.H., Sheridan, J., 2015. Moving model analysis of the slipstream ad wake of a high-speed train. J. Wind Eng. Ind. Aerodyn. 136, 127–137.

Bell, J.R., Burton, D., Thompson, M.C., Herbst, A.H., Sheridan, J., 2016a. Flow topology and unsteady features in the wake of a generic high-speed train. J. Fluids Struct. 61, 168–183.

Bell, J.R., Burton, D., Thompson, M.C., Herbst, A.H., Sheridan, J., 2016b. Dynamics of trailing vortices in the wake of a generic high-speed train. J. Fluids Struct. 65, 238–256.

Bell, J.R., Burton, D., Thompson, M.C., Herbst, A.H., Sheridan, J., 2014. The effect of length to height ratio on the wake structure and surface pressure of a high-speed train. In: 19th Australasian Fluid Mechanics Conference (AMFC), Melbourne, Australia, 8–11 December, 2014.

CEN. European Committee for Standardization. Railway Applications - Aerodynamics — Part 4: Requirements and test procedures for aerodynamics on open track, CEN EN 14067-4, 2009.

ERA. European Rail Agency. EU Technical Specification For Interoperability Relating to the 'Rolling Stock' Sub-System of the Trans-European High-Speed Rail System (HS RST TSI), 2008. 232/EC.

DIN Standards Committee Railway/Normenausschuss Fahrweg und Schienenfahrzeuge (FSF). ⟨www.fsf.din.de⟩, 2014.

Hemida, H., Baker, C., Gao, G., 2014. The calculation of train slipstreams using large-eddy simulation. Proc. Inst. Mech. Eng. Part F: J. Rail Rapid Transp. 228 (1), 25–36.

Hooper, J.D., Musgrove, A.R., 1997. Reynolds stress, mean velocity, and dynamic static pressure measurement by a four-hole pressure probe. Exp. Thermal Fluid Sci. 15, 375–383.

Krajnović, S., Davidson, L., 2005. Influence of floor motions in wind tunnels on the aerodynamics of road vehicles. J. Wind Eng. Ind. Aerodyn. 93, 677–696.

Kwon, H., Park, Y., Lee, D., Kim, M., 2001. Wind tunnel experiments on korean high-speed trains using various ground simulation techniques. J. Wind Eng. Ind. Aerodyn. 89, 1179–1195.

Morel, T., 1980. Effect of base slant on flow in the near wake of an axisymmetric cylinder. Aeronaut. Q., 132–147.

Muld, T., Efraimsson, G., Hennigson, D.S., 2012a. Flow structures around a high-speed train extracted using proper orthogonal decomposition and dynamic mode decomposition. Proc. Inst. Mech. Eng. Part F: J. Rail Rapid Transp. 57, 87–97.

Muld, T., Efraimsson, G., Hennigson, D.S., 2012b. Mode decomposition and slipstream velocities in the wake of two high-speed trains. Int. J. Railw. Technol. (submitted).

Muld, T., Efraimsson, G., Hennigson, D.S., 2013. Wake characteristics of high-speed trains with different lengths. Proc. Inst. Mech. Eng. Part F: Jo. Rail Rapid Transp. http://dx.doi.org/10.1177/0954409712473922 (published online), 2013.

Pii, L., Vanoli, E., Polidoro, F., Gautier, S., Tabbal, A., 2014. A full scale simulation of a high speed train for slipstream prediction. In: Proceedings of the Transport Reserach Arena, Paris, France.

Pope, C.W., 2007. Effective management of risk from slipstream effects at trackside and platforms. Rail Safety and Standards Board - T425 Report, 2007.

Sima, M., Tietze, A., Schulz, B., Ehrenfried, K., 2016. Representing large boundary layers in slipstream moving model tests. In: Proceedings of the Third International Conference on Railway Technology: Research, Development and Maintenance, Paper 50, 2016.

Sterling, M., Baker, C.J., Jordan, S.C., Johnson, T., 2008. A study of the slipstreams of high-speed passenger trains and freight trains. Proc. Inst. Mech. Eng. Part F: J. Rail Rapid Transp. 222, 177–193.

Weise, M., Schober, M., Orellano, A., 2006. Slipstream velocities induced by trains. In: Proceedings of the WSEAS International Conference on Fluid Mechanics and Aerodynamics, Elounda, Greece, 2006.